Postprint of: Wysocka J., Cieślik M., Krakowiak S., Ryl J., Carboxylic acids as efficient corrosion inhibitors of aluminium alloys in alkaline media, ELECTROCHIMICA ACTA, Vol. 289 (2018), pp. 175-192, DOI: 10.1016/j.electacta.2018.08.070

Carboxylic acids as efficient corrosion inhibitors of aluminium alloys in alkaline media

J. Wysocka, M. Cieslik, S. Krakowiak, J. Ryl*

Department of Electrochemistry, Corrosion and Materials Engineering, Gdansk University of Technology, Narutowicza St. 11/12, 80-233 Gdansk, Poland.

Corresponding author: jacek.ryl@pg.edu.pl

Abstract

The efficiency of AA5754 aluminium alloy corrosion inhibition achieved with maleic, malic, succinic, tartaric, citric, tricarballylic acids and serine in alkaline environment (pH 11) was examined. Selected corrosion inhibitors are characterized by different numbers and distribution of carbonyl and hydroxyl groups within their molecules. We have proposed and verified a novel approach for determining the adsorption isotherms based on the impedance measurements in galvanostatic mode (g-DEIS), allowing to distinguish subtle changes in the adsorption dynamics. It was shown that g-DEIS precisely determines the inhibitor concentration required for the full coverage of aluminium surface with the adsorbed inhibitor monolayer. Our approach was then cross-verified with the ellipsometry, cyclic polarization and classic EIS measurements, while the SEM and XPS analyses served to determine changes in the surface topography and chemistry. We have demonstrated that the investigated compounds significantly decelerate the corrosion rate of AA5754 at low inhibitor concentrations. Inhibition efficiency exceeds 99% at 6.9 mM for tricarballylic, 8.1 mM for citric and 12.0 mM for tartaric acid. The inhibition efficiency was primarily dependent on the high number of carbonyl groups in the molecule, while the inhibition provided by monocarboxylic amino acid (serine) was negligible, reaching 60% at 20 mM. The plotted isotherms fitted the Langmuir adsorption model, with similar values of Gibbs free energy for each studied inhibitor. The adsorption of carboxylic acids onto the surface of aluminium occurred via ligand exchange mechanism. On the basis of electrochemical and XPS studies, we claim that the role played by hydroxyl groups is secondary, while their presence slightly worsens the corrosion resistance of aluminium.

Keywords: AA5754 alloy, corrosion inhibitor, dynamic electrochemical impedance spectroscopy, carboxylic acids

1. Introduction

Aluminium and its alloys owe their high corrosion resistance to thin passive layer of Al_2O_3 [1], a process that occurs spontaneously as a result of the reaction with oxygen present in the air or dissolved in electrolytic environment. The passive layer is thermodynamically stable in the pH range between 4 and 9; exceeding this range results in a metal corrosion [2,3]. In alkaline environments, for pH > 9, the corrosion rate is controlled by the anodic dissolution of metal to $Al(OH)_4^-$ ions [4] through three main factors related to the kinetics of electrode reaction, mass transport and conductivity of passive layer on the metal surface [5–7]. The mechanism of aluminium corrosion in alkaline solutions can be divided into two competitive processes on the metal surface, i.e. direct metal dissolution and electrochemical formation/dissolution of aluminium hydroxide layer. The first process is characterized by high intensity, which translates directly into high corrosion rates. With progressing exposure of aluminium to an alkaline solution, $Al(OH)_3$ starts to limit the diffusion rate of ions reducing the corrosion rate [4,6,8]. Furthermore, the corrosion rate of aluminium in alkaline solutions is greatly influenced by physico-chemical properties of the environment, such as temperature, pH, conductivity etc. Detailed information on the corrosion mechanism of aluminium and its alloys in alkaline environments can be found in [9–14].

The enhanced corrosion rate of aluminium and its alloys in alkaline environments is a serious problem that significantly hinders the application potential of these materials. For example, the utilization of aluminium from batteries and fuel cells constituting an energy source for electric and hybrid vehicles [7,15–18]. The alkaline corrosion of aluminium is also a common problem for the industry, where the chemical cleaning agents used for removing contaminants from metal surfaces often have pH above 11. This is frequently observed, among others, in the paper industry (elements of printing presses) as well as in the transport industry (radiators).

Numerous inorganic and organic compounds were investigated with regard to their corrosion inhibition efficiency in aluminium. For instance, Macdonald and English [19] revealed the corrosion inhibition properties of SnO_3^{2-}, $Ga(OH)_4^-$, $In(OH)_3$, MnO_4^{2-}, BiO_3^{3-}. Awad et al. [20,21] investigated phosphates and chromates in strongly alkaline environments to determine the use of these compounds as metal passivators. The authors did not find high inhibitor efficiency for phosphates, most likely due to the very high pH value that was unfavorable for the formation of phosphate passive layer. Chromates revealed some corrosion inhibition properties at high concentrations, while at low concentrations, these compounds catalyzed the corrosion processes. Among the organic corrosion inhibitors, tributyl cerium phosphate [22–24], benzotriazole [25], 8-hydroxyquinoline [26–28], 2-mercaptobenzothiazole [29–31] and sodium benzoate [32] are the most frequently studied compounds. The inhibition efficiency for each of these compounds was reported to exceed 90%, while the inhibition mechanism is connected to the adsorption of functional groups such as C=O, C=S on a metal surface. The studies carried out by Amin et al. [33] on selected polyacrylic acids in alkaline solutions revealed similar inhibition mechanism in case of the aforementioned polymers. The

corrosion inhibition efficiency increased with increasing inhibitor concentration, molecular weight of the compound and exposure time.

Among the large group of organic compounds, citric acid is one of the most efficient corrosion inhibitors with regard to aluminium and its alloys in aqueous alkaline environments [34–37]. The reduction in corrosion rate is based on the strong complexing properties of Al^{3+} ions and the formation of chelate complexes [34,38–40]. Müller showed the inhibition effect of citric acid acting as aluminium pigment in waterborne paints [34]. Solmaz et al. [41] studied the inhibition properties of citric acid in high-purity aluminium (99.99%) in 2 M NaCl at pH 2, revealing an increase in inhibition efficiency up to a critical concentration of $1 \cdot 10^{-5}$ M. Above this critical concentration, the corrosion inhibition efficiency decreased. Similar studies were carried out by Kiyak and Kabasakaloğlu [42], who concluded that the electrochemical and chemical reactions associated with the dissolution of aluminium and precipitation reactions are competitive and depend directly on the pH of the solution, presence of a buffer, and polarization scan rate. Further improvement in the corrosion inhibition properties of citric acid was studied by Sarangapani et al. [43]. Their studies proved that among numerous inorganic compounds only metal oxides that stimulate the formation of anions (i.e. ZnO_2, As_2O_3, Al_2O_3) can also increase the corrosion inhibition efficiency in alkaline environments. Efficiency of carboxylic acids as corrosion inhibitors of aluminium alloys depends on inhibitor concentration and electrolyte pH. The maximum efficiency should be observed below Al_2O_3 isoelectric point, at pH < 9 [34,38].

A detailed study on the interaction of citric acid with AA5754 alloy in a bicarbonate buffer at pH 11 was also presented by Wysocka et al. [37] who proposed a novel approach towards constructing the adsorption isotherms based on the instantaneous impedance spectra analysis in galvanostatic mode (g-DEIS). The critical concentration of citric acid, sufficient to obtain full coverage of aluminium surface with the adsorbed monolayer at pH 11, was determined to be approx. 9 mM. The verification of the obtained results by using classic corrosion studies allowed the authors to conclude that the proposed methodology is an effective and valuable tool for monitoring the adsorption process on metal surfaces.

The interaction of citric acid with the aluminum surface, leading to the formation of complex compounds, occurs via two terminal carboxyl groups and the hydroxyl group [38,44]. Therefore, it can be assumed that other compounds classified as carboxylic acids and their derivatives should also exhibit inhibitory activity. Yurt et al. [45] performed calculations of the inhibitory efficiency of six amino acids (glycine, aspartic acid, valine, alanine, phenylalanine and glutamic acid) at pH 5, and six hydroxycarboxylic acids (glycolic acid, malic acid, lactic acid, mandelic acid, benzyl acid, citric acid) at pH 8. The authors also investigated the correlation between an experimentally-indiced pitting corrosion resistance and the molecule properties, such as electric charge density on active centers, dipole moment or highest occupied energy (HOMO) and the lowest uncluttered molecular orbital (LUMO). The authors concluded that physical adsorption and chemical adsorption play a key role in inhibiting the pitting corrosion of aluminum by the investigated corrosion

inhibitors. Based on the quantum calculations, it was stated that hydroxycarboxylic acids are donors and the amino acids are acceptors of free electron pair during the adsorption process.

The relationship between the structure of carboxylic acid and its inhibition properties was further elucidated in the work of Moussa et al. [46] on aromatic and aliphatic carboxylic acids. In the case of aromatic compounds, the inhibition efficiency depends, to a large extent, on the number and position of carboxyl groups as well as the presence of other substituents in the aromatic ring. The corrosion inhibition of aliphatic carboxylic acids increases with increasing carbon chain length. Brito and Sequeira [36] studied the electrochemical behavior of pure aluminium in the presence of various carboxyl acids, amino acids and quaternary amines. The authors concluded that most of these compounds are efficient corrosion inhibitors in alkaline environments. Based on the analysis of globally pooled results, the authors derived the following sequence of tested organic compounds in terms of decreasing efficiency: quaternary amines > amino acids > organic acids. The corrosion inhibition efficiency of organic acids increases with increasing number of carboxyl groups, although lactic and malic acids did not exhibit inhibition properties under test conditions. The present work provides a detailed investigation of the corrosion inhibition efficiency offered by selected tricarboxylic and dicarboxylic acids as well as serine, a monocarboxylic amino acid. The studies were carried out in a bicarbonate buffer at pH 11. The research goal was to investigate to what extent the subtle structural changes, such as the amount and distribution of the carboxyl and hydroxyl groups, and the presence of unsaturated bonds or amino groups affect the corrosion inhibition efficiency of carboxylic acids. Our secondary aim was to further verify the previously proposed method for adsorption isotherm estimation, which is based on the dynamic impedance measurements in galvanostatic mode (g-DEIS) during progressive injection of corrosion inhibitor. Monitoring of instantaneous impedance changes offers a unique possibility to distinguish even subtle changes in the electrochemical behavior of the investigated aluminium alloy.

2. Experimental

2.1 Sample preparation

Samples were prepared from commercial purity AA5754 alloy. The alloy's chemical composition was verified by means of Energy Dispersive X-Ray Spectroscopy (EDS). Alloy additives in wt.% were as follows: 3.6 % Mg, 0.5 % Mn, 0.3 % Fe, 0.3 % Si and 0.1 % Cr. The samples had cylindrical shape, 10 mm in diameter and 5 mm in thickness. After being cut from a rod, each sample underwent mechanical treatment, i.e. grinding (waterproof abrasive papers SiC 600 and 1500) and polishing (diamond suspension 6 and 1 μm with a mirror finish on 0.05 μm silica). This pretreatment was carried out on Digiprep 251 (Metkon, Turkey). Finally, the samples were rinsed in demineralized water, degreased in acetone, dried and enclosed in capsules made of PEEK, assuring their electric contact. The electrochemically exposed surface area was 0.5 cm^2. The SEM and EDS studies revealed two primary types of metal precipitates that form micro-galvanic cells with the

aluminium alloy matrix, i.e. anodic Mg_2Si and cathodic AlFe(Cr,Mn) (see Fig. 1.) The anodic phase in particular had the high susceptibility to undergo oxidation processes, even when exposed to atmospheric air [47].

2.2 Inhibitor compounds

The planned research was performed on a group of selected dicarboxylic and tricarboxylic acids and serine, each having similar structural formula. The primary goal was to discover the direct effect that various functional groups have on the corrosion inhibition efficiency, in order to further assess and possibly enhance the corrosion protection mechanism displayed by this group of organic compounds. For this purpose, compounds having different numbers of hydroxyl, carboxyl and amine groups were utilized. Citric acid was used as a reference in these studies, since it is known that it offers outstanding corrosion inhibition properties with regard to aluminium alloys in alkaline media [37]. The full list of investigated compounds, with their acronyms used in this work, is presented in Table 1.

From now on, the acronyms given in Table 1 will be used to label the investigated inhibitor compounds. Its arrangement is the following: *NAME(XY)*, where the numbers in brackets represent the amount of X – carboxyl and Y – hydroxyl groups in the molecule of investigated organic compound.

2.3 Dynamic impedance measurements for the construction of adsorption isotherms

The determination of an adsorption isotherm is one of the most commonly used procedures for studying the thermodynamic effect of the corrosion inhibitor interaction with the protected metal surface; it is primarily employed to investigate inhibitors displaying the anodic and mixed protection mechanism [48–50]. The construction of the adsorption isotherm is based on the analysis of inhibitor interaction with metal and the efficiency of corrosion rate reduction at a given concentration of inhibitor. In the corrosion studies, it is assumed that the surface coverage with adsorbent θ is equal to the inhibition efficiency of adsorbate $IE_{\%}$. The adsorption isotherms can be estimated from the electrochemical (both DC and AC techniques) [37,49], volumetric [51], or even gravimetric studies [48,52]. Each of them holds certain advantages and disadvantages, however, neither allows for (i) the estimation of inhibitor concentration that is sufficient for a full metal surface coverage with the adsorbed inhibitor monolayer, nor for (ii) the calculation of instantaneous changes in the inhibitory effect with varying concentration of corrosion inhibitor.

The determination of dynamic instantaneous changes in the investigated system as a result of corrosion inhibitor interaction solves this problem. Such assessment can be implemented by means of Dynamic Electrochemical Impedance Spectroscopy (DEIS), an approach proposed by Darowicki [53] and successfully used for investigating highly non-stationary electrochemical and corrosion processes [47,54–56]. The approach employs the idea of introducing a perturbation into the investigated system via a package of simultaneous multiple signals in a wide range of frequencies. The response signal is then processed within the so-called analysis window, required to locate the impedance spectrum obtained from Fourier

Transformation in the time domain. Therefore, during the DEIS measurements the system must remain stationary for as long as the length of the analysis window, which is typically between 1 and 10 seconds. Furthermore, the measurements can be carried out on-line and superimposed with the DC polarization techniques [57,58].

The DEIS approach allows for the determination of both the above-mentioned properties through impedance data analysis in the time domain, with ascending inhibitor concentration as an independent variable. Drawing the adsorption isotherm is based on estimation of inhibition efficiency through monitoring of instantaneous changes in charge transfer resistance R_{CT} with reference to R_{CT}^0 value in the absence of corrosion inhibitor:

$$IE_{\%} = \left(1 - \frac{R_{CT}^0}{R_{CT}}\right) * 100\% \quad (1)$$

Furthermore, the dynamic impedance analysis also allows for designating the inhibitor concentration that is sufficient for a full coverage of metal surface with the inhibitor. A detailed description of this operation is given in Section 3.3.

The basic obstacle encountered during the DEIS measurements is the alteration of the corrosion potential value E_{corr} due to the injection of corrosion inhibitor. It is known that in case of anodic corrosion inhibitors, when the inhibitory effect is provided by a direct or indirect passivation process, E_{corr} shifts towards more positive values. This is illustrated in Fig. 2 for each investigated inhibitor compound. The concentration of corrosion inhibitor that offers higher inhibitor efficiency can be already roughly estimated on the basis of changing E_{corr}, given that the injection rate of the corrosion inhibitor is known.

This feature has forced us to conduct the measurements in the galvanostatic mode under zero current conditions, j_{DC} = 0 in order to avoid the imposition of additional polarization components onto the investigated object. The causality condition of the impedance measurements would have been broken otherwise, hindering the proper comparison of various inhibitor compounds. Dynamic Electrochemical Impedance Spectroscopy in galvanostatic mode (g-DEIS) was implemented for the first time by Ryl et al. [47,59] to study cavitation erosion-corrosion phenomenon, where the corrosion potential was shifted under erosion exposure by up to 300 mV and the generated polarization currents led to a decrease in R_{CT} by two orders of magnitude. A similar approach has also been successfully employed in our previous studies on corrosion inhibitors [37].

2.4 Dynamic impedance setup and measurements

The corrosion studies were carried out by means of a setup consisting of two cells connected with a peristaltic pump, described in details in previous study [37]. The electrochemical measurements were carried out in a corrosion cell in the absence of corrosion inhibitor for the first 1000 s and then at its increasing concentrations. A three-electrode setup was used with the investigated aluminium alloy as a working

electrode (WE), $Ag|Ag_2O$ as a reference electrode (RE) (E^0 = +0.174 V vs SHE), and the platinum mesh as a counter electrode (CE). Peristaltic pump PP 1-05 (Zalimp, Poland) was set to dose the corrosion inhibitor from the secondary cell to the corrosion cell at a constant flow rate of 0.37 mL/min. The concentration of investigated corrosion inhibitor in the secondary cell was selected in such a way as to assure that its concentration in the corrosion cell will be 20 mM at the end of a 6000 s long experiment. The primary electrolyte was bicarbonate buffer (pH 11) prepared from 0.05 M $NaHCO_3$ + 0.1 M NaOH. The initial electrolyte volume in the corrosion cell was 350 mL.

As previously mentioned, the DEIS measurements were conducted in galvanostatic mode (g-DEIS) under zero DC current. The system setup for impedance measurements was composed of Autolab PGSTAT 128N (Metrohm, Netherlands) potentiostat/galvanostat connected to two measurement cards, namely, PXI-4464 for the generation of AC signal, and PXI-6124 for the acquisition of AC/DC signals. The aforementioned cards were operating in PXIe-1073 chassis (all from National Instruments, USA). The g-DEIS measurements were performed using multisinusoidal perturbation signal composed of 30 elementary signals of various frequencies in the range between 4.5 kHz and 0.5 Hz, with 8 points per decade of frequency. The sampling frequency was 128 kHz. The phase shifts and amplitudes of each elementary signal were adjusted individually by optimization software written in LabView environment to ensure that the resulting peak-to-peak amplitude of multisinusoidal signal meets the linearity condition of impedance measurements. It has been assumed that the amplitude of response signal cannot exceed 20 mV. Additionally, a voltage divider was used to adjust perturbation amplitude throughout the measurement in order to take into consideration substantial changes in current-voltage dependence as a result of inhibitor injection. Upon registration, the acquisition signal was sequenced with an analysis window 10 s in length, and subjected to Fourier Transformation. A similar approach was successfully adopted in previous g-DEIS studies [37,47]. Details on the fundamentals of DEIS methodology can be found elsewhere [53,60,61].

2.5 Supporting corrosion studies

Supporting electrochemical measurements, i.e. cyclic polarization (CP) and electrochemical impedance spectroscopy (EIS) were carried out by means of Gamry Reference 600+ potentiostat (Gamry Instruments, USA) for cross-verification purposes. Each sample was conditioned for 20 minutes prior to its examination for this purpose. EIS measurements were carried out in potentiostatic mode using sinusoidal perturbation signal with a frequency range between 10 kHz and 100 mHz, in descending order. The peak-to-peak amplitude of each sinusoidal signal was 15 mV. CP scans were recorded in the polarization range between -0.25 vs E_{corr} and +2.00 V vs $Ag|Ag_2O$. The scan rate was 2 mV/s.

2.6 Microscopic and spectroscopic surface analysis

The physico-chemical examination of inhibition efficiency provided by the studied corrosion inhibitors as well as various forms of interaction between the metal and inhibitor compound was carried out by means of scanning electron microscopy (SEM), energy dispersive X-ray spectroscopy (EDS), X-ray photoelectron spectroscopy (XPS) and ellipsometry. SEM microscope S-3400N (Hitachi, Japan) was used for surface degradation analysis in the microscopic scale. It was equipped with a tungsten filament and operated in secondary electron mode, at 20 kV. The microscope was expanded with EDS detector UltraDry (ThermoFisher Scientific, USA) for the examination of surface chemistry. Furthermore, high-resolution XPS analyses were performed on Escalab 250Xi (ThermoFisher Scientific, USA), equipped with a monochromatic AlKα source. These measurements were carried out at 10 eV pass energy and an energy step size of 0.05 eV. The X-ray spot was 250 μm. Charge compensation was assured through flood gun, while the final calibration was carried out by shifting the X-axis (binding energy, BE) for peak characteristics of adventitious carbon 1s at 284.6 eV. Proper peak differentiation was verified using *Al2p3* peak for metallic aluminium, measured on AA5754 prior to electrochemical studies as reference (72.7 eV).

The ellipsometry measurements were performed by using single wavelength ellipsometer ELX-02C (DRE, Germany) operating 632.8 nm laser at 70° angle of incidence. These measurements were carried out on-line during the electrochemical studies at variable concentrations of corrosion inhibitor in the 80 mL electrochemical cell (Horiba, France).

3. Results and discussion

3.1 Corrosion measurements

A series of g-DEIS measurements were performed by injecting a corrosion inhibitor and monitoring instantaneous changes in the resulting impedance spectra. The exemplary spectra in Nyquist projection are presented in Fig. 3a-c for serine as well as succinic and citric acids, the latter two being the representatives of di- and tricarboxylic acids, respectively. In each case, time is marked on the Z-axis, where the first 1000 s served for initial sample conditioning in bicarbonate buffer (pH 11), followed by the injection of corrosion inhibitor from the secondary cell. The shape of impedance spectra for serine are changing only slightly, which is equivalent to a small change in the corrosion inhibition efficiency. On the other hand, the remaining samples showed a significant increase in impedance loop radius over time, typically after 3000 to 4500 s into the experiment (2000 to 3500 s after the inhibitor injection).

The knowledge about the instantaneous value of corrosion inhibitor concentration at any given time point and the recorded instantaneous impedance spectra allow for a precise determination of inhibitor/metal interaction. In order to perform such analysis, it is essential to fit the impedance data by using an electric equivalent circuit (EEC). The above task is particularly challenging when taking into consideration the dynamic changes in equilibrium at the metal's interface and the necessity to consider both boundary cases

with such a circuit, i.e. active corrosion in the absence of inhibitor, and the occurrence of protective adsorbed layer in the presence of inhibitor. EEC must also reflect the true values (and their changes) of the real components. The most adequate EEC is presented in Fig. 4a, where it consists of two parallel sub-circuits. The first sub-circuit characterizes the adsorbed protective layer formed by the corrosion inhibitor, while the second one describes electrochemical processes on the active surface. The surface coverage is represented by θ, and thus the active area is denoted as (1-θ). This EEC was successfully applied by Juttner [62] and Mansfeld [63] to analyze the pitting corrosion in aluminium. Its application for this study is limited due to two factors, i.e. dynamically changing value of θ and the restricted frequency range of g-DEIS measurements [61]. Furthermore, due to the dielectric character of adsorbed inhibitor layer, its electrical resistance is relatively high and not taking part in charge transfer, and thus can be omitted. The limitation of frequency range to ~1 Hz also neglects the impact of diffusion transport represented by the Warburg element. Usually, the restriction of impedance spectra in the frequency domain is a disadvantage of DEIS-based techniques. However, it allows for further simplification of EEC to the form presented in Fig. 4b. The actual shape of the impedance spectra, presented in Figs 3a-c, reveals the heavy overlapping of both time-constants in the frequency domain. This phenomenon results in the increase in capacitance dispersion. The capacitance dispersion is described by the surface distribution model, representing the surface areas of different electric properties on the metallic surface of aluminium. The main contributor to the capacitance dispersion is the dynamically changing surface coverage with the investigated corrosion inhibitor, as visualized in Fig. 4d. Therefore, due to time-constant overlapping, the EEC may be further simplified to singular time-constant circuit, with a constant phase element (CPE) placed instead of capacitance, R(QR), in order to properly consider the capacitance dispersion factor. Such EEC representation is often found in similar studies [1,58,64–66]. The impedance of CPE is given by eq. (2), and it represents a combination of the adsorbed inhibitor layer capacitance and double layer capacitance.

$$Z_{CPE} = [Q(j\omega)^n]^{-1} \quad (2)$$

It is worth noting that the exponent *n* is the measure of surface heterogeneity. For an ideal capacitor, *n* = 1. In such case, its behavior will, to a large extent, depend on the degree of surface coverage (see Fig. 4d), as demonstrated later in the paper.

Figure 4e presents changes in the resultant charge transfer resistance R_{CT} at the metal/electrolyte interface obtained on the basis of g-DEIS instantaneous spectra which were analyzed with R(QR) EEC. Thus, the application of g-DEIS allows for precise determination of the corrosion inhibition efficiency for any given concentration of corrosion inhibitor throughout the measurement by monitoring the latter parameter. In order to do so, the inhibitor concentration was plotted on the X-axis for the known concentration and flow rate of inhibitor from the secondary cell (0.37 mL/min). Data plotted in Fig. 4e confirmed that in case of both tricarboxylic acids the concentration required to achieve the pronounced increase in charge transfer resistance at the metal/electrolyte interface was the lowest among the investigated compounds. Both

tricarboxylic acids displayed almost a three orders of magnitude increase in the value of R_{CT} for concentrations below 10 mM, followed by all the dicarboxylic acids being equally efficient (< 15 mM). Here, an increase in R_{CT} for succinic and maleic acids is significantly higher than for malic and tartaric acids, possibly because of the absence of hydroxyl groups in the structure of the inhibitor molecule. The least effective was serine, which is a monocarboxylic amino acid. A slow but continuous increase in R_{CT} was observed as a result of serine injection. A simple observation can be made that the compounds having the same number of carboxylic groups act very much alike, while the influence resulting from the presence of hydroxyl groups is small.

In order to verify the g-DEIS approach, classic corrosion studies were also performed by means of electrochemical impedance spectroscopy (EIS) and cyclic polarization measurements (CP). In order to verify the g-DEIS approach, classic corrosion studies were also performed by means of electrochemical impedance spectroscopy (EIS) and cyclic polarization measurements (CP). Neither of these can be performed under dynamically changing electrolytic conditions, thus two inhibitor concentrations (4.5 and 20 mM) were used to compare results. More detailed CP, EIS and g-DEIS comparison for citric acid is presented elsewhere [37]. The measurements obtained from the EIS and CP analyses are presented in Fig. 5 and Fig. 6, respectively.

The analysis of EIS and g-DEIS spectra was carried out using the same R(QR) EEC at the same frequency range. The EIS results are much more scattered in the low frequency range due to non-stationary conditions during the active corrosion of aluminium (c = 4.5 mM). This behavior was previously described in literature [14,66]. Nevertheless, the highest corrosion inhibitor efficiency of tricarballylic acid, manifested by the biggest impedance loop at c = 4.5 mM, confirms that a very low concentrations of this compound is sufficient to reduce the corrosion rate. At higher inhibitor concentration, both tricarboxylic acids performed the best, while the effect of serine was negligible. The values of impedance parameters and inhibitor efficiency obtained with the g-DEIS and EIS techniques for the inhibitor concentrations of 4.5 and 20 mM are presented in Table 2.

The cyclic polarization curves presented in Fig. 6 show the current-voltage dependence for aluminium alloys exposed to bicarbonate buffer, and how the addition of selected inhibitors affects these curves due to the corrosion inhibition process. In the case of electrolytic measurements in the absence of corrosion inhibitor, the current stabilizes at 10^{-3} A cm^{-2} after the initial period of active metal dissolution. The stabilization of current density is related to the formation of the corrosion product layer, as evidenced by the lowered current density with increasing anodic polarization. The polarization curves obtained in the presence of the investigated carboxylic acids revealed a reduction in current density in the passive state. The compounds having two carboxyl groups per molecule showed smaller change in current in the passive state compared to the compounds with three carboxyl groups, while serine at a concentration of 4.5 mM had a very small inhibitory effect. The processes associated with formation of the corrosion product layer and adsorbed inhibitor molecules layer are competitive at low inhibitor concentrations, as demonstrated on the base of

SEM and XPS studies [37]. Energetic surface heterogeneity due to the presence of corrosion products islands for low adsorbate concentrations usually translates to stronger adsorption. It can be assumed that the presence of a corrosion product layer will positively influence the formation of the protective adsorbate layer. An increase in the inhibitor concentration up to 20 mM significantly reduced the aluminium corrosion rate for each investigated dicarboxylic and tricarboxylic acid. The current density in the passive state was less than 10^{-5} A cm^{-2}, and the value of this parameter was again lower for tricarboxylic acids. The inhibition efficiency, $IE_{\%}$ was calculated using the Tafel extrapolation procedure [67–70]. The obtained values increased from approx. 60 to over 97% due to the increased inhibitor concentration.

The differences between various corrosion studies should be attributed to the different forms of system perturbation and susceptibility of the EIS and CP measurements to non-stationary conditions. Furthermore, cyclic polarization does not provide direct information on the electrochemical process occurring at the metal/electrolyte interface, while the corrosion rate may only be estimated using the Tafel extrapolation approach, a transformation of Butler-Volmer equation. The error increases in the presence of adsorbed or passive layers [71,72]. EIS allows the assessment of both the mechanism and the kinetics of the corrosion process in certain cases. The analysis requires to maintain the stationary conditions as well as linear current-voltage dependence during polarization, otherwise the shape of impedance spectra is affected. Furthermore, similarly to g-DEIS, it requires the analysis by means of EEC. The g-DEIS method also requires the fitting procedure but allows us to measure the changes in instantaneous values of electric parameters as often as every few seconds, and unaffected by non-stationary conditions. Its major flaw is the restricted frequency range, where is it difficult to characterize the processes with very high relaxation times, such as diffusion or charge transfer through organic coatings [73]. Corrosion products may start to form during sample conditioning when proposed measurement procedure is used. This might have an influence on the adsorption mechanism. If observed, restriction of sample conditioning duration is advised.

Table 2 contains the values of inhibition efficiency for the investigated carboxylic acids that had been determined via three different measuring techniques, i.e. g-DEIS, EIS and CP. The differences between the inhibition efficiencies estimated with each technique are particularly noticeable at low inhibitor concentrations (under non-stationary conditions), and close to negligible at high inhibitor concentrations.

3.2 Microscopic and spectroscopic analyses

The scanning electron microscopy (SEM) micrographs confirmed the diversity of surface failures in the materials exposed to various carboxylic acids. The micrographs also revealed a similar behavior in the case of compounds having the same number of carboxylic groups. For this reason, Fig. 7 shows only selected and representative micrographs, resulting from 6000 s exposure to bicarbonate buffer containing 4.5 and 20 mM of corrosion inhibitor. As expected from the outcome of impedance studies, the lower inhibitor concentration of 4.5 mM was not sufficient to form a full coverage with the adsorbed inhibitor molecules on

the surface of aluminium alloy. At the same time, the corrosion attack was mild and mostly proceeded in the direct vicinity of intermetallic particles, affecting the surroundings of AlFe(Cr,Mn) particles that are cathodic in respect to the alloy matrix (Fig. 7a,b). The failure was more severe in the presence of serine compared to any of the carboxylic acids. It is also worth noting that in case of dicarboxylic acids, the lowest amount of material loss at the inhibitor concentration of 4.5 mM was observed for succinic acid. On the other hand, the anodic Mg_2Si phase was not notably influenced within the time of exposure, which is likely due to the thermodynamic stability of $Mg(OH)_2$ in alkaline media, shifting the corrosion potential of Mg_2Si phase towards more cathodic potentials [74]. The high concentration of Mg within this phase was confirmed by the EDS analysis. The similar influence of microstructure on the corrosion behavior of aluminium alloys is well documented for various environments displaying mild corrosive hazard [75–78].

For both tricarboxylic acids in question, represented by citric acid in Fig. 7c, the local corrosion of intermetallic particles may be neglected. At the same time, much higher surface coverage by the inhibitor compounds is clearly visible in the SEM images in the form of large dark areas. The nature of these areas was initially confirmed by the EDS technique (EDS map of carbon in the inset of Fig. 7c) and later on, by XPS. A number of studies revealed the possibility of a catalytic effect at such low concentration of anodic corrosion inhibitor due to the formation of passive-active galvanic cells between the areas with and without the adsorbed passive layer [78–80]. This scenario was not observed in the case of investigated carboxylic acids, as confirmed by the g-DEIS measurements where increased inhibition efficiency was already notable at low inhibitor concentrations.

The SEM micrographs registered after exposure to the buffer containing 20 mM di- or tri-carboxylic acid did not reveal any surface corrosion failure, either general or in the vicinity of galvanic microcells formed by the microstructure. Both anodic Mg_2Si and cathodic AlFe(Cr,Mn) particles were unaffected. Thus, the corrosion studies suggesting that 20 mM is the sufficient inhibitor concentration to enable wide corrosion protection have been confirmed. The situation is different in the case of serine (see Fig. 7d), where the general corrosion process was already limited, but the chemistry as well as the topography of surrounding intermetallic particles have been altered. While serine offers some input into corrosion inhibition efficiency, it is significantly lower than that of dicarboxylic and tricarboxylic acids. For each investigated dicarboxylic acid, the corrosion inhibitor concentration required to form the adsorbed monolayer is higher than that of tricarboxylic acids (refer to Fig. 4d). Thus, we came to the conclusion that in the case of monocarboxylic serine, its critical concentration might be even higher. Therefore, we performed another experiment employing the corrosion inhibitor concentrations up to 100 mM. However, the obtained inhibition efficiency was not visibly improved. At the same time, the surface of aluminium alloy exposed to 100 mM serine became covered with various forms of agglomerated species, as can be seen in the inset of Fig. 7d. The most likely explanation of this phenomenon is the effect occurring in surfactants and related to the critical (maximum) inhibitor concentration, which is not higher than CMC [81–83]. Therefore, it can be assumed that

serine cannot efficiently form the protective adsorbed passive layer in a wide range of applied concentrations, or the formed layer does not offer the barrier properties.

High-resolution XPS spectra were measured in the binding energy (BE) range of *C1s*, *O1s*, *Al2p3* and *Mg1s* photopeaks in order to determine the interaction types between the studied inhibitor compounds and the aluminium alloy surface. The analysis was performed after exposure to the electrolyte containing 20 mM of corrosion inhibitor, as in the case of microstructural analysis by SEM. The aim of the performed analysis was the qualitative and quantitative comparison of various chemical species present at the metal/electrolyte interface and the determination of inhibition mechanism. The XPS results are presented in Fig. 8 and Table 3.

The deconvolution of XPS spectra within *C1s* BE range was performed using three primary components to distinguish the chemistry characteristics of organic corrosion inhibitors [37,84]. The primary component, present at BE of 286.2 $\pm$ 0.2 eV, is attributable to C-O bonds. The second component, most visible in the case of both tricarboxylic acid and succinic acid, is strongly shifted towards higher values, ranging between +2.9 and up to +4.2 eV, which is characteristic for C=O bond in ester, carbonyl and carboxyl functional groups. Finally, C-C/C-H aliphatic bonds were deconvoluted at 285.1 eV. For each investigated inhibitor compound, the adsorbed layer formed on the aluminium surface was mainly composed of C-O bonds whose contribution was not always the same. For tricarboxylic acids and succinic acid, the share of C-O bonds was the highest, exceeding 25 at.%, while it remained relatively high for the rest of dicarboxylic acids, with an exception of maleic acid. For the remaining two inhibitors in question, the C-C to C-O ratio observed on the aluminium surface was much higher, revealing the altered chemistry of the adsorbed layer. Contrary to serine, the high concentration of C-C aliphatic bonds in maleic acid did not translate into low inhibition efficiency. For the serine sample, a small peak appeared at 287.7 eV, which is attributable to the C-N bonds of amine groups.

The high-resolution XPS spectra measured within *O1s* energy range were also composed of three individual components, whose presence is often observed on the surface of metal samples [80,85–88]. The main component (identified as OH/CO) was located at 532.8 $\pm$ 0.2 eV. It is most frequently attributed to the surface hydroxyl groups of aluminium, and also to oxygen in carbonyl or ester groups that were expected within the adsorbed passive layer formed in the presence of the studied corrosion inhibitors. Further distinction between the various species analyzed within *O1s* OH/CO peak was possible after applying the estimation proposed by McCafferty and Wightman [88]. This approach was proposed in the studies on the determination of surface hydroxyl group concentration in metal oxides. The contribution from the carbonyl and hydroxyl groups can be quantified by using eq. (3-5).

$$I_{CO}^{O1s} = \frac{I_{CO}^{C1s}}{I_{CC}^{C1s} + I_{CO}^{C1s} + I_{C=O}^{C1s}} * \left(\frac{at.\%C}{at.\%O}\right) * I_{OH/CO}^{O1s} \quad (3)$$

$$I_{C=O}^{O1s} = \frac{I_{C=O}^{C1s}}{I_{CC}^{C1s} + I_{CO}^{C1s} + I_{C=O}^{C1s}} * \left(\frac{at.\%C}{at.\%O}\right) * I_{OH/CO}^{O1s} \quad (4)$$

$$I_{OH}^{O1s} = I_{OH/CO}^{O1s} - \left(I_{CO}^{O1s} + I_{C=O}^{O1s}\right) \quad (5)$$

where I_x^y is the contribution from the given type of bond *X*, quantified by using one of photopeaks, *Y*: *O1s* or *C1s*, while *at.%C* and *at.%O* are the overall contributions of carbon and oxygen. Thus, the contribution from the hydroxyl groups can be estimated by subtracting the results from eq. (3) and (4) from the total intensity of *O1s* OH/CO photopeak, as presented in eq. (5).

The outcome of the aforementioned estimation is presented in Table 3. It is clearly visible that according to the suggested mechanism of inhibition provided by carboxylic acids, the highest inhibition efficiency corroborates the highest contribution from C-O bonds and also from carbonyl bonds. For both tricarboxylic acids in question, their shared amount exceeded 26%. The third highest amount of adsorbed C-O and C=O species was observed for succinic acid, which is also in good agreement with the observed corrosion inhibition efficiency. In the case of maleic acid, the high share of hydroxyl groups should be connected to the electrophilic addition of water to unsaturated bonds in the presence of H^+ ions. Naturally, the smallest area of *O1s* peak attributable to C-O and C=O bonds was observed for monocarboxylic serine. Here, a small 1.0 % contribution from nitrogen in amine groups (BE of 400.2 eV in *N1s* peak [89]) was also included. The results corroborate previous findings on aromatic carboxylic acids in alkaline environment, connecting the inhibition efficiency with the adsorption of carbonyl groups on the aluminium surface and their electron density [46]. Furthermore, the lower the inhibition efficiency, the higher the contribution from aluminium hydroxide species on the analyzed sample surface, which is direct evidence for lower corrosion resistance in the presence of a specific investigated compound.

The remaining two components of *O1s* spectral deconvolution were ascribed to the metal oxide species O^{2-}, shifted by -1.1 eV, and the chemisorbed water within the layer, shifted by +1.6 eV with regard to the major OH/CO peak. According to the literature review, the peak position of OH- and O^{2-} species are typically 1.1 to 1.5 eV apart [87,88]. When comparing the chemistry of the adsorbed layer formed on aluminium by citric acid interaction in alkaline environment, Wysocka et al. [37] observed that the amount of chemisorbed water is the highest for actively corroding samples compared to the samples protected by corrosion inhibitor. The authors explained this observation by the higher hydration of nonstoichiometric corrosion products. A similar finding was observed in the present study, based on the comparison with the results obtained for the reference sample exposed to bicarbonate buffer (pH 11) only. A decrease in the amount of chemisorbed water on the metal surface is in good agreement with the ligand exchange mechanism of adsorption [38,90]. The amount of chemisorbed water varied among different inhibitors (from 1.6 to even 4.7 %), however, it did not reach the highest value for serine as would be expected on the basis of corrosion studies. On the other hand, the lowest amount of metal oxide species was recorded for both tricarboxylic acids displaying the highest corrosion resistance, which corroborates previous findings [37].

No significant differences were recorded in the chemistry of *Al2p3* peak for the investigated di- and tricarboxylic acids; each *Al2p3* peak was composed of two peak doublets located at 72.8 and 75.3 ± 0.1 eV. These peak doublets are typically associated with the metallic aluminium (Al_m) and its naturally grown Al_2O_3

(Al_{ox1}). The presence of Al_m peak indicates small thickness of formed adsorption layer, not exceeding 10 nm, due to limited depth of XPS signal acquisition. The Al_m:Al_{ox1} ratio for the aforementioned samples was similar, ranging between 0.3:1 and 0.6:1, which suggests a negligible difference in the layer thickness. The serine sample revealed significant differences, with the Al_m peak missing and the Al_{ox1} peak shifted by +0.8 eV. This feature marks the appearance of non-stoichiometric corrosion products on the surface of aluminium exposed to alkaline environment and is yet another proof of the low inhibition efficiency of serine [14]. Thick films, with thickness exceeding 10 nm, conceal the contribution of metallic Al. The broadening and positive BE shift of oxide peaks within the nonstoichiometric corrosion product layer (Al_{ox2}) together with concealed Al_m contribution were also confirmed in the present studies for the reference sample measurements in the absence of corrosion inhibitor.

It is important to note that plausible errors in the XPS analysis result from the aluminium contact with atmospheric air followed by the formation of naturally grown Al_2O_3 passive layer as well as atmospheric contamination with adventitious carbon [78,91]. These side effects were only partially limited by the short duration of sample storage between the corrosion tests and XPS examination, while sample etching prior to the XPS measurements was not possible due to the very small thickness of the investigated layers.

3.3 Adsorption isotherms for various carboxylic acids on the aluminium alloy surface

One of the primary conditions required to construct an adsorption isotherm is that the maximum concentration used should not exceed the concentration for which the adsorbed species form a full monolayer coverage on the metal surface [92]. This condition is particularly difficult to meet when using classic corrosion measurements, such as the gravimetric or cyclic polarization measurements. During our previous studies on citric acid, we claimed that the g-DEIS approach surpasses classical tools of analysis in this regard [37] because the exact determination of inhibitor concentration necessary for the formation of 3D adsorbed layer can be achieved through instantaneous monitoring of capacitance changes. The resulting capacitance C of the investigated surface is described by eq. (6):

$$C = \frac{\varepsilon_0 \varepsilon_r A}{d} \tag{6}$$

where, A is the investigated surface area, d is layer thickness, and ε_0 and ε_r are the electric constant and the relative static permittivity, respectively. According to the SEM micrographs presented in Fig. 7, none of the samples displayed significant variation of surface area due to the corrosion process. The material loss was measurable only in case of serine. Since the value of dielectric constant for thin adsorbed layers is very similar with regard to a bicarbonate buffer and the investigated carboxylic acids, the primary component affecting the layer's capacitance is the thickness of this layer. Also, the direct determination of the optical constants of dielectric films from the ellipsometry measurements is not possible for very thin layers (< 10 nm thickness) [93].

In this study, due to spatial heterogeneity of the electrode throughout the exposure time, the electric double layer capacitance is represented by the constant phase element (CPE) in accordance with eq. (2). The exponent *n* in this equation is a measure of surface heterogeneity. For solid electrodes immersed in aqueous solutions, the typical n values range between 0.7 and 0.9, depending on the factors such as roughness and porosity, intermetallic particles, adsorbed layers etc. [47,94,95]. In order to determinate the concentration of corrosion inhibitor that is sufficient for the formation of the adsorbed monolayer, c_{3D}, an effective capacitance C_{eff} need to be estimated on the basis of CPE parameters. Hirschorn et al. [96] proposed such a model for the surface distribution of time constants. Thus, C_{eff} can be estimated by using eq. (7):

$$C_{eff} = Q^{1/n}\left(\frac{R_e R_{ct}}{R_e + R_{ct}}\right)^{(1-n)/n} \tag{7}$$

Monitoring the effective capacitance changes is assumed to be sufficient for the determination of c_{3D}. To confirm this assumption, we performed the single-wavelength ellipsometry measurements, which can be carried out *in situ* via g-DEIS while a peristaltic pump injects the corrosion inhibitor into the corrosion cell. Therefore, the ellipsometry measurements enabled the cross-verification of both procedures. The determination of layer's thickness on the basis of ellipsometry typically requires a fitting procedure by using the measured ellipsometric angles Δ and ψ [97,98]. However, for thin films of few angstroms, such as the ones observed on the polished metal surfaces, the increase in thickness can be easily estimated *on-line* by using the Drude approximation [93,99]. The approximation states that the change in Δ ellipsometry angle is proportional to the thickness of the investigated film, as expressed in eq. (8):

$$\delta\Delta^0 = \Delta^0 - \Delta = C_\Delta d \tag{8}$$

where, Δ^0 is the film-free value for Δ and C_Δ is the proportionality constant. For films which are only few angstroms thick, it is said that the change in Δ is more important than its absolute value [93]. Conveniently, the value of Δ measured at the start of the experiment on aluminium immersed in the bicarbonate buffer at pH 11 can be approximated by Δ^0, since aluminium oxides are not thermodynamically stable in this pH range. In Fig. 9, using citric acid as an example, the changes in effective capacitance C_{eff} calculated from the impedance studies using CPE as well as the changes in $\delta\Delta^0$ measured via single-wavelength ellipsometry are presented. The capacitance value was only slightly affected by the citric acid addition in the amount equal up to the inhibitor concentration of 7.5 mM, and it showed a very abrupt drop at concentrations > 7.5 mM. It was previously speculated that the observed drop is correlated to the increase in the adsorbed layer thickness (refer to eq. (8)) [37]. This hypothesis has been validated by the changes in $\delta\Delta^0$. Due to the very high sensitivity of ellipsometry, it was possible to confirm that there was virtually no increase in the layers thickness at the beginning of the experiment. The observed small variation of $\delta\Delta^0$ should be connected to the formation of 2D inhibitor monolayers on the aluminium alloy surface and the hydrogen reduction reaction in the very early stage of the experiment. Furthermore, a gradual yet significant increase in $\delta\Delta^0$ precisely coincides with the decreased value of effective capacitance parameter. The aforementioned

conclusion is also in good agreement with the observed changes in the CPE exponent *n* (at the top of Fig. 9), which at first showed large variation due to the instantaneous formation of "isles" consisting of 2D adsorbed corrosion inhibitor, with dynamically changing size and stability. However, once the inhibitor fully covered the metal surface in the form of a monolayer, the electrochemical homogeneity on the surface increased, giving an effect in stabilization and increased *n* values. This observation is of particular importance because it also shows that the continuous monitoring by using DEIS/g-DEIS allows for the determination of changes in the surface homogeneity throughout the process.

A similar approach was applied for all the remaining corrosion inhibitors in order to estimate the critical concentration of a given compound that is sufficient for the formation of 3D adsorbed monolayer on the aluminium alloy surface. The changes in C_{eff} with varying inhibitor concentration are presented in Fig. 10, while the values of c_{3D} are summarized in the table contained in the same figure.

We suggest the use of term inhibition yield to describe the lowest inhibitor concentration, which is sufficient for significant increase of inhibition efficiency, here connected to full coverage of protected metal surface with adsorbed inhibitor layer. Such optimal inhibitor concentration is often bound to CMC [100,101]. It is clear that the concentration sufficient for the formation of adsorbed monolayer on the surface of aluminium alloy is much lower for both investigated tricarboxylic acids and it does not exceed 8 mM. In the case of the investigated dicarboxylic acids, the c_{3D} values are similar and in the range of 12-13 mM. It can thus be concluded that the tricarboxylic acids not only possess higher inhibition efficiency, resulting from the charge transfer resistance and Tafel extrapolation measurements, but they are also characterized by higher inhibition yield, being able to form the adsorbed monolayer at lower inhibitor concentrations.

At very low corrosion inhibitor concentrations, i.e. below c_{3D}, the behavior of each carboxylic acid is very similar and characterized by the stable value of effective capacitance, or its slow increase. This feature is most likely related to the gradual change of relative static permittivity within the electric double layer, small differences in the double layer capacitance among the investigated samples and, to a lesser extent, the variation of the electrolyte temperature ($\pm$ 1 °C). On the other hand, when the adsorbed monolayer is already formed, the influence of inhibitor concentration on the effective capacitance is negligible, suggesting negligible differences in the structure of forming adsorbed layers.

Among many different types of adsorption isotherms used in the corrosion inhibitor studies, the Langmuir isotherm adsorption model is most frequently employed in relation to aluminium alloys [102–106]. Its primary conditions are: (i) adsorbate molecules attach to the active sites of the adsorbent surface, (ii) the maximum possible level of adsorption corresponds to the formation of adsorbate monolayer, and (iii) all active sites are equally valuable and the adsorbed molecules do not interact with each other thus the adsorption energy should be constant regardless of surface coverage. The second aforementioned condition is the hardest to fulfill in the corrosion studies, and is the primary advantage of the g-DEIS approach, as explained earlier. The more complex adsorption models take into consideration factors such as the surface

heterogeneity and the presence of areas having different adsorption energy (Temkin isotherm [104]) or interactions between the adsorbed molecules (Frumkin isotherm [103]). However, it is fundamental to realize that the adsorption isotherm provides information about the resultant heat effect of all the processes occurring at the adsorbent/adsorbate interface, including but not restricted to sorption, hydration or dissolution processes. Therefore, the exact determination of individual input from each process in electrolytic environment is impossible. Furthermore, the non-linear behavior of the proposed isotherm may result from failure to comply with the second assumption of Langmuir isotherm. This example was previously evidenced in the case of citric acid studies in alkaline media [37].

The Langmuir adsorption isotherms were plotted for each investigated corrosion inhibitor on the basis of instantaneous R_{CT} values obtained from the g-DEIS measurements, as presented in Fig. 11a. The isotherms were drawn for the corrosion inhibitor concentration not exceeding the concentration at which the formation of adsorbed inhibitor monolayer occurs, i.e. $c_{inh} \leq c_{3D}$ (refer to inset of Fig. 10), which was different for each investigated compound. The linear behavior of surface coverage $log(\theta/1-\theta)$ plotted against the corrosion inhibitor concentration $log(c_h)$ confirmed that the investigated compounds interacting with the aluminium metal surface follow the Langmuir adsorption isotherm model. Furthermore, high density of data points in these plots was also very time-efficient thanks to the g-DEIS approach, thus offering the improved accuracy in the process of deriving a general equation for the isotherm. Fig. 11b presents the same results obtained by using the same approach, however, without the limiting condition of maximum concentration, c_{3D}. The slope of linear function obtained in Fig. 11a corresponds to the logarithm of equilibrium constant $log(Kc)$ and thus allows for the determination of Gibbs free energy, ΔG by using eq. (9):

$$\Delta G = -RTln(Kc) \tag{9}$$

where, c is the molar concentration of water (55.5 M). The obtained ΔG values for each investigated inhibitor are summarized in Table 4.

The negative ΔG values allow for the conclusion that for each investigated corrosion inhibitor, its interaction with the aluminium surface in a bicarbonate buffer is spontaneous in nature [107,108]. It should be emphasized that the adsorption mechanism for all investigated corrosion inhibitors is similar, as proved by small variation in ΔG values. The values of free Gibbs energy not exceeding -20 kJ mol^{-1} are often reported in case of physical adsorption mechanism, where the binding forces are purely electrostatic. More negative ΔG values are typical for chemisorption and the formation of chemical bonds between filled π-orbitals in the oxygen atoms and partially unoccupied π-orbitals in the *d*-block metals. Therefore, in this particular case, it is difficult to clearly distinguish between the two adsorption mechanisms, as follows: (i) due to the excess of negative charge on aluminium surface, adsorption between an electron and the donor carbonyl group, further connected to negatively charged oxygen atom, is not highly plausible, and (ii) pure chemisorption is also unlikely due to large electropositivity and the lack of *d* orbitals involved in the formation of chemical bonds with an inhibitor molecule. Therefore, it is most likely that the reduction in the corrosion rate

mediated by carboxylic acids can be described by the ligand exchange model, as a result of creating coordination compounds embedded in the hydrated oxide layer on the metal surface. The coordination compound is formed between the organic acid anions contained in the electrolyte and Al^{3+} cations resulting from the metal dissolution. Chemisorption mechanism may only occur on the adsorbed layer of metal oxides rather than directly on the metal surface. It is worth noting that the abrupt increase in isotherm slope after the monolayer formation (see Fig. 11b) indicates an increase in chemisorption effect and the formation of thicker layer with better barrier properties [109], further confirmed by the ellipsometry studies (refer to Fig. 9). The resulting inhibition efficiency will, to a large extent, depend on the sequestration of Al^{3+} cations. This adsorption mechanism is also applicable in relation to serine (ΔG = -20.71 kJ/mol). The adsorption process is possible from the thermodynamic point of view, and has been confirmed by the XPS analysis. Amine groups are electrophilic, thus can be adsorbed chemically and physically onto the aluminium surface. Being bidentate ligands, amino acids can also be described by the ligand exchange model. However, the ligand exchange is not highly efficient in the case of amine groups, as observed in the electrochemical and XPS studies.

The following sequence describes the investigated compounds taking into consideration the inhibition yield, from highest to lowest:

CAR(30) > CIT(31) > [TAR(22) = MAL(21) = SUC(20) = MAE(20)] > SER(11).

The corrosion inhibition efficiency varied with the corrosion inhibitor concentration; the variation was most pronounced at concentrations not exceeding c_{3D}. It was observed that both the inhibition efficiency and inhibition yield are primarily related to the adsorption of carbonyl –C=O groups on the metal surface and significantly increases with increasing number of carbonyl groups per inhibitor molecule. High inhibition efficiency is provided by tricarboxylic acids even at low inhibitor concentrations, as a result. The differences in $IE_{\%}$ may thus be related to the electron density of the carbonyl groups as well as the size of the molecules [46,110]. These results corroborate the studies by Sarangapani et al. [111] on citric, succinic, malic and lactic acids.

In contrast to the carbonyl groups, the presence and number of hydroxyl groups in the inhibitor molecule do not significantly alter either corrosion inhibition efficiency at high inhibitor concentrations or inhibition yield. Tricarballylic acid, which does not contain the hydroxyl groups, is characterized by a slightly lower c_{3D} value, while its inhibition efficiencies at concentrations exceeding c_{3D} are almost the same. Compared to tricarballylic acid, the presence of hydroxyl group in citric acid shifts the isoelectric point of alumina by almost one unit of pH further into the acidic area, affecting the pH in the vicinity of aluminium surface as well as decreasing the molecule mobility. The inhibition yields of all analyzed dicarboxylic acids are very similar. However, the highest inhibition efficiency at concentrations exceeding c_{3D} was observed for succinic acid, which does not contain the hydroxyl groups.

4. Conclusions

We have clearly demonstrated that the increase in the corrosion inhibition efficiency due to the presence of carboxylic acid is primarily connected to the amount of carbonyl groups per inhibitor molecule. Aluminium protected by any of the investigated tricarboxylic acids, namely, tricarballylic acid or citric acid, was characterized by the highest measured values of charge transfer resistance, with each technique challenged only by succinic acid in the g-DEIS measurements.

The adsorption isotherms plotted for each investigated compound displayed the similar values of Gibbs free energy, ranging between -21 and -17 kJ/mol, which demonstrated the same mechanism of the adsorbed layer formation. It was postulated that the protection mechanism is based on the ligand exchange mechanism. The similarity of the structure and thickness of each layer formed by di- and tricarboxylic acids was also confirmed by the effective capacitance monitoring, XPS and the ellipsometry studies at high inhibitor concentrations. The adsorption layer was primarily composed of C-O bonds, as revealed by the XPS analysis. On the other hand, the layer formed by inhibitors with higher corrosion resistance had significant contribution from the carboxyl and carbonyl groups present in its structure. It was also revealed that the formation of adsorbed layer is preceded by a decrease in the amount of chemisorbed water on the metal surface. This finding corroborates the proposed ligand exchange mechanism of adsorption that affects barrier properties offered by the layer.

The higher the number of carbonyl groups, the better the corrosion inhibition effect. However, the increased number of carbonyl groups also had an effect on the inhibition yield, allowing for more effective formation of the adsorbed monolayer at lower inhibitor concentrations due to the sequestration of Al^{3+} ions. The critical inhibitor concentration, c_{3D}, which is sufficient for a full coverage with the adsorbed monolayer, was the lowest for tricarballylic acid (approx. 6.5 mM) and citric acid (approx. 8.0 mM), i.e. ca. two times lower than for any dicarboxylic acid.

The amino acid serine offered the lowest inhibition efficiency by far. While the thermodynamics of the serine adsorption process was similar to that of other investigated compounds, the adsorbed serine layer was not offering comparable barrier properties and inhibition efficiency. The presence of only one carbonyl group in the serine molecule is the most likely reason for this. The amine group of serine does not improve the amino acid's complexing properties and chelate formation.

The effect due to the presence and number of hydroxyl groups in the inhibitor molecule is secondary compared to the carbonyl group contribution. However, the XPS studies revealed that the most efficient inhibitors had the lowest number of hydroxyl groups on the aluminium surface. It was also observed that succinic and maleic acids, which do not have the hydroxyl groups in their molecules, displayed better inhibition efficiency than malic and tartaric acids. Furthermore, citric acid showed lower inhibition yield compared to tricarballylic acid. The only difference between these two acids is the absence of hydroxyl group in tricarballylic acid. This subtle variation in the structure of inhibitor molecule did not alter its inhibition

efficiency at concentrations above 10 mM. For each investigated corrosion inhibitor, an increase in its concentration in a bicarbonate buffer led to the improved inhibition efficiency. This feature is not always the case for anodic corrosion inhibitors, where the presence of active-passive galvanic microcells may cause an increase in the corrosion rate at low inhibitor concentrations.

5. Acknowledgments

Authors are grateful to Prof. Pawel Slepski for consultation and assistance with respect to the modification of impedance measurement methodology. Authors acknowledge the financial support of the Polish Ministry of Science and Higher Education from the budget funds in the period 2016-2019 under Iuventus Plus project IP2015067574.

6. References

[1] J.H.W. de Wit, H.J.W. Lenderink, Electrochemical impedance spectroscopy as a tool to obtain mechanistic information on the passive behaviour of aluminium, Electrochim Acta. 41 (1996) 1111–1119. doi:10.1016/0013-4686(95)00462-9.

[2] C.R. Werrett, D.R. Pyke, A.K. Bhattacharya, XPS Studies of Oxide Growth and Segregation in Aluminium-Silicon Alloys, Surf. Interface Anal. 25 (1997) 809–816. doi:10.1002/(SICI)1096-9918(199709)25:10<809::AID-SIA304>3.0.CO;2-M.

[3] S. Feliu, M.J. Bartolomé, Influence of alloying elements and etching treatment on the passivating films formed on aluminium alloys, Surf. Interface Anal. 39 (2007) 304–316. doi:10.1002/sia.2456.

[4] J. Zhang, M. Klasky, B.C. Letellier, The aluminum chemistry and corrosion in alkaline solutions, J. Nucl. Mater. 384 (2009) 175–189. doi:10.1016/j.jnucmat.2008.11.009.

[5] S. Adhikari, K.R. Hebert, Participation of Aluminum Hydride in the Anodic Dissolution of Aluminum in Alkaline Solutions, J. Electrochem. Soc. 155 (2008) C189. doi:10.1149/1.2883827.

[6] D. Chu, R.F. Savinell, Experimental data on aluminum dissolution in KOH electrolytes, Electrochimica Acta. 36 (1991) 1631–1638. doi:10.1016/0013-4686(91)85017-2.

[7] M.L. Doche, J.J. Rameau, R. Durand, F. Novel-Cattin, Electrochemical behaviour of aluminium in concentrated NaOH solutions, Corros. Sci. 41 (1999) 805–826. doi:10.1016/S0010-938X(98)00107-3.

[8] S.-I. Pyun, S.-M. Moon, Corrosion mechanism of pure aluminium in aqueous alkaline solution, J. Solid State Electrochem. 4 (2000) 267–272. doi:10.1007/s100080050203.

[9] H.B. Shao, J.M. Wang, Z. Zhang, J.Q. Zhang, C.N. Cao, Electrochemical impedance spectroscopy analysis on the electrochemical dissolution of aluminum in an alkaline solution, J. Electroanal. Chem. 549 (2003) 145–150. doi:10.1016/S0022-0728(03)00266-3.

[10] D.D. Macdonald, Evaluation of Alloy Anodes for Aluminum-Air Batteries, J. Electrochem. Soc. 135 (1988) 2410. doi:10.1149/1.2095348.

[11] R.D. Armstrong, V.J. Braham, The mechanism of aluminium corrosion in alkaline solutions, Corros. Sci. 38 (1996) 1463–1471. doi:10.1016/0010-938X(96)00037-6.

[12] K.C. Emregül, A.A. Aksüt, The behavior of aluminum in alkaline media, Corros. Sci. 42 (2000) 2051–2067. doi:10.1016/S0010-938X(00)00055-X.

[13] I. Boukerche, S. Djerad, L. Benmansour, L. Tifouti, K. Saleh, Degradability of aluminum in acidic and alkaline solutions, Corros. Sci. 78 (2014) 343–352. doi:10.1016/j.corsci.2013.10.019.

[14] J. Wysocka, S. Krakowiak, J. Ryl, K. Darowicki, Investigation of the electrochemical behaviour of AA1050 aluminium alloy in aqueous alkaline solutions using Dynamic Electrochemical Impedance Spectroscopy, J. Electroanal. Chem. 778 (2016) 126–136. doi:10.1016/j.jelechem.2016.08.028.

[15] S.H. Yang, H. Knickle, Modeling the performance of an aluminum–air cell, J. Power Sources. 124 (2003) 572–585. doi:10.1016/S0378-7753(03)00811-5.

[16] S. Yang, Design and analysis of aluminum/air battery system for electric vehicles, J. Power Sources. 112 (2002) 162–173. doi:10.1016/S0378-7753(02)00370-1.
[17] X. Zhang, S.H. Yang, H. Knickle, Novel operation and control of an electric vehicle aluminum/air battery system, J. Power Sources. 128 (2004) 331–342. doi:10.1016/j.jpowsour.2003.09.058.
[18] Q. Li, N.J. Bjerrum, Aluminum as anode for energy storage and conversion: a review, J. Power Sources. 110 (2002) 1–10. doi:10.1016/S0378-7753(01)01014-X.
[19] D.D. Macdonald, C. English, Development of anodes for aluminium/air batteries ? solution phase inhibition of corrosion, J. Appl. Electrochem. 20 (1990) 405–417. doi:10.1007/BF01076049.
[20] K.M. Kamel, S.A. Awad, A. Kassab, Non-corrosive action of the tertiary phosphate ion on aluminium, J. Electroanal. Chem. Interfacial Electrochem. 127 (1981) 195–202. doi:10.1016/S0022-0728(81)80478-0.
[21] S.A. Awad, K.M. Kamel, A. Kassab, Effect of anions on the corrosion of aluminium in sodium, J. Electroanal. Chem. Interfacial Electrochem. 127 (1981) 203–209. doi:10.1016/S0022-0728(81)80479-2.
[22] D. Ho, N. Brack, J. Scully, T. Markley, M. Forsyth, B. Hinton, Cerium Dibutylphosphate as a Corrosion Inhibitor for AA2024-T3 Aluminum Alloys, J. Electrochem. Soc. 153 (2006) B392. doi:10.1149/1.2217260.
[23] S.J. García, T.H. Muster, ö. Özkanat, N. Sherman, A.E. Hughes, H. Terryn, J.H.W. de Wit, J.M.C. Mol, The influence of pH on corrosion inhibitor selection for 2024-T3 aluminium alloy assessed by high-throughput multielectrode and potentiodynamic testing, Electrochimica Acta. 55 (2010) 2457–2465. doi:10.1016/j.electacta.2009.12.013.
[24] S.J. Garcia, T.A. Markley, J.M.C. Mol, A.E. Hughes, Unravelling the corrosion inhibition mechanisms of bi-functional inhibitors by EIS and SEM–EDS, Corros. Sci. 69 (2013) 346–358. doi:10.1016/j.corsci.2012.12.018.
[25] M.L. Zheludkevich, K.A. Yasakau, S.K. Poznyak, M.G.S. Ferreira, Triazole and thiazole derivatives as corrosion inhibitors for AA2024 aluminium alloy, Corros. Sci. 47 (2005) 3368–3383. doi:10.1016/j.corsci.2005.05.040.
[26] W. Liu, A. Singh, Y. Lin, E.E. Ebenso, L. Zhou, B. Huang, 8-Hydroxyquinoline as an effective corrosion inhibitor for 7075 aluminum alloy in 3.5% NaCl solution, Int. J. Electrochem. Sci. 9 (2014) 5574–5584.
[27] S. Marcelin, N. Pébère, Synergistic effect between 8-hydroxyquinoline and benzotriazole for the corrosion protection of 2024 aluminium alloy: A local electrochemical impedance approach, Corros. Sci. 101 (2015) 66–74. doi:10.1016/j.corsci.2015.09.002.
[28] H.N. Soliman, Influence of 8-hydroxyquinoline addition on the corrosion behavior of commercial Al and Al-HO411 alloys in NaOH aqueous media, Corros. Sci. 53 (2011) 2994–3006. doi:10.1016/j.corsci.2011.05.045.
[29] A.C. Balaskas, M. Curioni, G.E. Thompson, Effectiveness of 2-mercaptobenzothiazole, 8-hydroxyquinoline and benzotriazole as corrosion inhibitors on AA 2024-T3 assessed by electrochemical methods: Evaluation of inhibitors on AA 2024-T3 by electrochemical methods, Surf. Interface Anal. 47 (2015) 1029–1039. doi:10.1002/sia.5810.
[30] S.V. Lamaka, M.L. Zheludkevich, K.A. Yasakau, M.F. Montemor, M.G.S. Ferreira, High effective organic corrosion inhibitors for 2024 aluminium alloy, Electrochimica Acta. 52 (2007) 7231–7247. doi:10.1016/j.electacta.2007.05.058.
[31] T.G. Harvey, S.G. Hardin, A.E. Hughes, T.H. Muster, P.A. White, T.A. Markley, P.A. Corrigan, J. Mardel, S.J. Garcia, J.M.C. Mol, A.M. Glenn, The effect of inhibitor structure on the corrosion of AA2024 and AA7075, Corros. Sci. 53 (2011) 2184–2190. doi:10.1016/j.corsci.2011.02.040.
[32] W.B.W. Nik, O. Sulaiman, S.G.E. Giap, R. Rosliza, Assessment of Sodum Benzoate Corrosion Inhibitor on AA6063 in Wate, Biosci. Biotechnol. Res. Asia. 10 (2013) 637–643. doi:10.13005/bbra/1175.
[33] M.A. Amin, S.S.A. EI-Rehim, E.E.F. El-Sherbini, O.A. Hazzazi, M.N. Abbas, Polyacrylic acid as a corrosion inhibitor for aluminium in weakly alkaline solutions. Part I: Weight loss, polarization, impedance EFM and EDX studies, Corros. Sci. 51 (2009) 658–667. doi:10.1016/j.corsci.2008.12.008.
[34] B. Müller, Citric acid as corrosion inhibitor for aluminium pigment, Corros. Sci. 46 (2004) 159–167. doi:10.1016/S0010-938X(03)00191-4.
[35] B. Müller, K. Franze, D. Mebarek, Corrosion Inhibition of Aluminum Pigments in Aqueous Alkaline Media at Different pH Values, CORROSION. 51 (1995) 625–630. doi:10.5006/1.3293623.
[36] P.S.D. Brito, C.A.C. Sequeira, Organic Inhibitors of the Anode Self-Corrosion in Aluminum-Air Batteries, J. Fuel Cell Sci. Technol. 11 (2013) 011008. doi:10.1115/1.4025534.

[37] J. Wysocka, S. Krakowiak, J. Ryl, Evaluation of citric acid corrosion inhibition efficiency and passivation kinetics for aluminium alloys in alkaline media by means of dynamic impedance monitoring, Electrochimica Acta. 258 (2017) 1463–1475. doi:10.1016/j.electacta.2017.12.017.
[38] P.C. Hidber, T.J. Graule, L.J. Gauckler, Citric Acid-A Dispersant for Aqueous Alumina Suspensions, J. Am. Ceram. Soc. 79 (1996) 1857–1867. doi:10.1111/j.1151-2916.1996.tb08006.x.
[39] M. Katoh, Influence of chelating agent (citric acid) and F− on corrosion of Al, Corros. Sci. 8 (1968) 423–431. doi:10.1016/S0010-938X(68)90084-X.
[40] A.K. Powell, S.L. Heath, X-ray structural analysis of biologically relevant aluminium(III) complexes, Coord. Chem. Rev. 149 (1996) 59–80. doi:10.1016/S0010-8545(96)90012-0.
[41] R. Solmaz, G. Kardaş, B. Yazıcı, M. Erbil, Citric acid as natural corrosion inhibitor for aluminium protection, Corros. Eng. Sci. Technol. 43 (2008) 186–191. doi:10.1179/174327807X214770.
[42] T. Kıyak, M. Kabasakaloğlu, The anodic behaviour of cathodically pretreated aluminum electrodes in 0.1 M NaCl solution containing citrate ion, Appl. Surf. Sci. 140 (1999) 24–32. doi:10.1016/S0169-4332(98)00339-0.
[43] K.B. Sarangapani, V. Balaramachandran, V. Kapali, S.V. Iyer, M.G. Potdar, K.S. Rajagopalan, Aluminium as anode in primary alkaline batteries. Influence of additives on the corrosion and anodic behaviour of 2S aluminium in alkaline citrate solution, J. Appl. Electrochem. 14 (1984) 475–480. doi:10.1007/BF00610812.
[44] P. Rubini, A. Lakatos, D. Champmartin, T. Kiss, Speciation and structural aspects of interactions of Al(III) with small biomolecules, Coord. Chem. Rev. 228 (2002) 137–152. doi:10.1016/S0010-8545(01)00467-2.
[45] A. Yurt, B. Duran, H. Dal, An experimental and theoretical investigation on adsorption properties of some diphenolic Schiff bases as corrosion inhibitors at acidic solution/mild steel interface, Arab. J. Chem. 7 (2014) 732–740. doi:10.1016/j.arabjc.2010.12.010.
[46] M.N. Moussa, M.M. El-Tagoury, A.A. Radi, S.M. Hassan, Carboxylic acids as corrosion inhibitors for aluminium in acidic and alkaline solutions, Anti-Corros. Methods Mater. 37 (1990) 4–8. doi:10.1108/eb007262.
[47] J. Ryl, K. Darowicki, P. Slepski, Evaluation of cavitation erosion–corrosion degradation of mild steel by means of dynamic impedance spectroscopy in galvanostatic mode, Corros. Sci. 53 (2011) 1873–1879. doi:10.1016/j.corsci.2011.02.004.
[48] A. Singh, I. Ahamad, M.A. Quraishi, Piper longum extract as green corrosion inhibitor for aluminium in NaOH solution, Arab. J. Chem. 9 (2016) S1584–S1589. doi:10.1016/j.arabjc.2012.04.029.
[49] A.M. Abdel-Gaber, E. Khamis, H. Abo-Eldahab, S. Adeel, Novel package for inhibition of aluminium corrosion in alkaline solutions, Mater. Chem. Phys. 124 (2010) 773–779. doi:10.1016/j.matchemphys.2010.07.059.
[50] N. Chaubey, V.K. Singh, M.A. Quraishi, Electrochemical approach of Kalmegh leaf extract on the corrosion behavior of aluminium alloy in alkaline solution, Int. J. Ind. Chem. 8 (2017) 75–82. doi:10.1007/s40090-016-0103-y.
[51] E.E. Oguzie, A.I. Onuchukwu, P.C. Okafor, E.E. Ebenso, Corrosion inhibition and adsorption behaviour of *Ocimum basilicum* extract on aluminium, Pigment Resin Technol. 35 (2006) 63–70. doi:10.1108/03699420610652340.
[52] N. Chaubey, V.K. Singh, Savita, M.A. Quraishi, E.E. Ebenso, Corrosion Inhibition of Aluminium Alloy in alkaline Media by Neolamarkia Cadamba Bark Extract as a Green Inhibitor, Int. J. Electrochem. Sci. 10 (2015) 504–518.
[53] K. Darowicki, Theoretical description of the measuring method of instantaneous impedance spectra, J. Electroanal. Chem. 486 (2000) 101–105. doi:10.1016/S0022-0728(00)00110-8.
[54] K. Darowicki, S. Krakowiak, P. Ślepski, Evaluation of pitting corrosion by means of dynamic electrochemical impedance spectroscopy, Electrochimica Acta. 49 (2004) 2909–2918. doi:10.1016/j.electacta.2004.01.070.
[55] S. Krakowiak, K. Darowicki, P. Slepski, Impedance investigation of passive 304 stainless steel in the pit pre-initiation state, Electrochimica Acta. 50 (2005) 2699–2704. doi:10.1016/j.electacta.2004.11.015.
[56] L. Burczyk, K. Darowicki, Determination of Local Corrosion Current from Individual Harmonic Components, J. Electrochem. Soc. 164 (2017) C796–C800. doi:10.1149/2.1001713jes.

[57] P. Slepski, K. Darowicki, K. Andrearczyk, On-line measurement of cell impedance during charging and discharging process, J. Electroanal. Chem. 633 (2009) 121–126. doi:10.1016/j.jelechem.2009.05.002.
[58] H. Gerengi, K. Darowicki, P. Slepski, G. Bereket, J. Ryl, Investigation effect of benzotriazole on the corrosion of brass-MM55 alloy in artificial seawater by dynamic EIS, J. Solid State Electrochem. 14 (2010) 897–902. doi:10.1007/s10008-009-0923-1.
[59] J. Ryl, J. Wysocka, P. Slepski, K. Darowicki, Instantaneous impedance monitoring of synergistic effect between cavitation erosion and corrosion processes, Electrochimica Acta. 203 (2016) 388–395. doi:10.1016/j.electacta.2016.01.216.
[60] K. Darowicki, P. Ślepski, Dynamic electrochemical impedance spectroscopy of the first order electrode reaction, J. Electroanal. Chem. 547 (2003) 1–8. doi:10.1016/S0022-0728(03)00154-2.
[61] J. Orlikowski, J. Ryl, M. Jarzynka, S. Krakowiak, K. Darowicki, Instantaneous Impedance Monitoring of Aluminum Alloy 7075 Corrosion in Borate Buffer with Admixed Chloride Ions, CORROSION. 71 (2015) 828–838. doi:10.5006/1546.
[62] K. Jüttner, Electrochemical Impedance Spectroscopy on 3-D Inhomogeneous Surfaces, J. Electrochem. Soc. 135 (1988) 332. doi:10.1149/1.2095610.
[63] F. Mansfeld, Electrochemical impedance spectroscopy (EIS) as a new tool for investigating methods of corrosion protection, Electrochimica Acta. 35 (1990) 1533–1544. doi:10.1016/0013-4686(90)80007-B.
[64] J.B. Bessone, D.R. Salinas, C.E. Mayer, M. Ebert, W.J. Lorenz, An EIS study of aluminium barrier-type oxide films formed in different media, Electrochimica Acta. 37 (1992) 2283–2290. doi:10.1016/0013-4686(92)85124-4.
[65] S. Gudić, J. Radošević, M. Kliškić, Impedance and transient study of aluminium barrier-type oxide films, J. Appl. Electrochem. 26 (1996) 1027–1035. doi:10.1007/BF00242197.
[66] F. Bentiss, M. Lebrini, M. Lagrenée, Thermodynamic characterization of metal dissolution and inhibitor adsorption processes in mild steel/2,5-bis(n-thienyl)-1,3,4-thiadiazoles/hydrochloric acid system, Corros. Sci. 47 (2005) 2915–2931. doi:10.1016/j.corsci.2005.05.034.
[67] C. Andrade, C. Alonso, Corrosion rate monitoring in the laboratory and on-site, Constr. Build. Mater. 10 (1996) 315–328. doi:10.1016/0950-0618(95)00044-5.
[68] A.D. King, N. Birbilis, J.R. Scully, Accurate Electrochemical Measurement of Magnesium Corrosion Rates; a Combined Impedance, Mass-Loss and Hydrogen Collection Study, Electrochimica Acta. 121 (2014) 394–406. doi:10.1016/j.electacta.2013.12.124.
[69] M. Curioni, F. Scenini, T. Monetta, F. Bellucci, Correlation between electrochemical impedance measurements and corrosion rate of magnesium investigated by real-time hydrogen measurement and optical imaging, Electrochimica Acta. 166 (2015) 372–384. doi:10.1016/j.electacta.2015.03.050.
[70] W.J. Lorenz, F. Mansfeld, Determination of corrosion rates by electrochemical DC and AC methods, Corros. Sci. 21 (1981) 647–672. doi:10.1016/0010-938X(81)90015-9.
[71] A.V. Sokirko, F.H. Bark, Diffusion-migration transport in a system with butler-volmer kinetics, an exact solution, Electrochimica Acta. 40 (1995) 1983–1996. doi:10.1016/0013-4686(94)00359-9.
[72] E. Leiva, P. Meyer, W. Schmickler, Electron transfer through passive films: Role of localized electronic states, Corros. Sci. 29 (1989) 225–236. doi:10.1016/0010-938X(89)90032-2.
[73] K. Darowicki, P. Ślepski, M. Szociński, Application of the dynamic EIS to investigation of transport within organic coatings, Prog. Org. Coat. 52 (2005) 306–310. doi:10.1016/j.porgcoat.2004.06.007.
[74] M. Pourbaix, R.W. Staehle, Lectures on Electrochemical Corrosion, Springer US, Boston, MA, 1973. http://dx.doi.org/10.1007/978-1-4684-1806-4 (accessed May 7, 2018).
[75] N. Birbilis, R.G. Buchheit, Electrochemical Characteristics of Intermetallic Phases in Aluminum Alloys, J. Electrochem. Soc. 152 (2005) B140. doi:10.1149/1.1869984.
[76] F. Zeng, Z. Wei, J. Li, C. Li, X. Tan, Z. Zhang, Z. Zheng, Corrosion mechanism associated with Mg2Si and Si particles in Al–Mg–Si alloys, Trans. Nonferrous Met. Soc. China. 21 (2011) 2559–2567. doi:10.1016/S1003-6326(11)61092-3.
[77] K.A. Yasakau, M.L. Zheludkevich, S.V. Lamaka, M.G.S. Ferreira, Role of intermetallic phases in localized corrosion of AA5083, Electrochimica Acta. 52 (2007) 7651–7659. doi:10.1016/j.electacta.2006.12.072.
[78] J. Ryl, J. Wysocka, M. Jarzynka, A. Zielinski, J. Orlikowski, K. Darowicki, Effect of native air-formed oxidation on the corrosion behavior of AA 7075 aluminum alloys, Corros. Sci. 87 (2014) 150–155. doi:10.1016/j.corsci.2014.06.022.

[79] A. Boag, A.E. Hughes, A.M. Glenn, T.H. Muster, D. McCulloch, Corrosion of AA2024-T3 Part I: Localised corrosion of isolated IM particles, Corros. Sci. 53 (2011) 17–26. doi:10.1016/j.corsci.2010.09.009.
[80] D.S. Kharitonov, C. Örnek, P.M. Claesson, J. Sommertune, I.M. Zharskii, I.I. Kurilo, J. Pan, Corrosion Inhibition of Aluminum Alloy AA6063-T5 by Vanadates: Microstructure Characterization and Corrosion Analysis, J. Electrochem. Soc. 165 (2018) C116–C126. doi:10.1149/2.0341803jes.
[81] A.M. Abdel-Gaber, B.A. Abd-El-Nabey, I.M. Sidahmed, A.M. El-Zayady, M. Saadawy, Inhibitive action of some plant extracts on the corrosion of steel in acidic media, Corros. Sci. 48 (2006) 2765–2779. doi:10.1016/j.corsci.2005.09.017.
[82] K. Xhanari, M. Finšgar, Organic corrosion inhibitors for aluminum and its alloys in chloride and alkaline solutions: A review, Arab. J. Chem. (2016). doi:10.1016/j.arabjc.2016.08.009.
[83] M. Elachouri, M.S. Hajji, M. Salem, S. Kertit, J. Aride, R. Coudert, E. Essassi, Some Nonionic Surfactants as Inhibitors of the Corrosion of Iron in Acid Chloride Solutions, CORROSION. 52 (1996) 103–108. doi:10.5006/1.3292100.
[84] I. Djordjevic, N.R. Choudhury, N.K. Dutta, S. Kumar, Synthesis and characterization of novel citric acid-based polyester elastomers, Polymer. 50 (2009) 1682–1691. doi:10.1016/j.polymer.2009.01.045.
[85] G. Yoganandan, J.N. Balaraju, Synergistic effect of V and Mn oxyanions for the corrosion protection of anodized aerospace aluminum alloy, Surf. Coat. Technol. 252 (2014) 35–47. doi:10.1016/j.surfcoat.2014.04.062.
[86] M. Amin, M. Saracoglu, N. El-Bagoury, T. Sharshar, M. Ibrahim, J. Wysocka, J. Ryl, Microstructure and Corrosion Behaviour of Carbon Steel and Ferritic and Austenitic Stainless Steels in NaCl Solutions and the Effect of p-Nitrophenyl Phosphate Disodium Salt, Int. J. Electrochem. Sci. 11 (2016) 10029–10052. doi:10.20964/2016.12.17.
[87] M. Giza, P. Thissen, G. Grundmeier, Adsorption Kinetics of Organophosphonic Acids on Plasma-Modified Oxide-Covered Aluminum Surfaces, Langmuir. 24 (2008) 8688–8694. doi:10.1021/la8000619.
[88] E. McCafferty, J.P. Wightman, Determination of the concentration of surface hydroxyl groups on metal oxide films by a quantitative XPS method, Surf. Interface Anal. 26 (1998) 549–564. doi:10.1002/(SICI)1096-9918(199807)26:8<549::AID-SIA396>3.0.CO;2-Q.
[89] N. Graf, E. Yegen, T. Gross, A. Lippitz, W. Weigel, S. Krakert, A. Terfort, W.E.S. Unger, XPS and NEXAFS studies of aliphatic and aromatic amine species on functionalized surfaces, Surf. Sci. 603 (2009) 2849–2860. doi:10.1016/j.susc.2009.07.029.
[90] R. Kummert, W. Stumm, The surface complexation of organic acids on hydrous γ-Al2O3, J. Colloid Interface Sci. 75 (1980) 373–385. doi:10.1016/0021-9797(80)90462-2.
[91] S. Evans, Correction for the effects of adventitious carbon overlayers in quantitative XPS analysis, Surf. Interface Anal. 25 (1997) 924–930. doi:10.1002/(SICI)1096-9918(199711)25:12<924::AID-SIA317>3.0.CO;2-2.
[92] R.I. Masel, Principles of adsorption and reaction on solid surfaces, Wiley, New York, 1996.
[93] H.G. Tompkins, W.A. McGahan, Spectroscopic ellipsometry and reflectometry: a user's guide, Wiley, New York, 1999.
[94] C.-H. Kim, S.-I. Pyun, J.-H. Kim, An investigation of the capacitance dispersion on the fractal carbon electrode with edge and basal orientations, Electrochimica Acta. 48 (2003) 3455–3463. doi:10.1016/S0013-4686(03)00464-X.
[95] J.-B. Jorcin, M.E. Orazem, N. Pébère, B. Tribollet, CPE analysis by local electrochemical impedance spectroscopy, Electrochimica Acta. 51 (2006) 1473–1479. doi:10.1016/j.electacta.2005.02.128.
[96] B. Hirschorn, M.E. Orazem, B. Tribollet, V. Vivier, I. Frateur, M. Musiani, Determination of effective capacitance and film thickness from constant-phase-element parameters, Electrochimica Acta. 55 (2010) 6218–6227. doi:10.1016/j.electacta.2009.10.065.
[97] R. Bogdanowicz, J. Ryl, K. Darowicki, B.B. Kosmowski, Ellipsometric study of oxide formation on Cu electrode in 0.1 M NaOH, J. Solid State Electrochem. 13 (2009) 1639–1644. doi:10.1007/s10008-008-0650-z.
[98] L.M.M. de Souza, F.P. Kong, F.R. McLarnon, R.H. Muller, Spectroscopic ellipsometry study of nickel oxidation in alkaline solution, Electrochimica Acta. 42 (1997) 1253–1267. doi:10.1016/S0013-4686(96)00298-8.

[99] A.N. Saxena, Changes in the Phase and Amplitude of Polarized Light Reflected from a Film-Covered Surface and Their Relations with the Film Thickness, J. Opt. Soc. Am. 55 (1965) 1061. doi:10.1364/JOSA.55.001061.
[100] V. Branzoi, F. Golgovici, F. Branzoi, Aluminium corrosion in hydrochloric acid solutions and the effect of some organic inhibitors, Mater. Chem. Phys. 78 (2003) 122–131. doi:10.1016/S0254-0584(02)00222-5.
[101] P. Karlsson, A.E.C. Palmqvist, K. Holmberg, Surface modification for aluminium pigment inhibition, Adv. Colloid Interface Sci. 128–130 (2006) 121–134. doi:10.1016/j.cis.2006.11.010.
[102] A.F.S. Abdul Rahiman, S. Sethumanickam, Corrosion inhibition, adsorption and thermodynamic properties of poly(vinyl alcohol-cysteine) in molar HCl, Arab. J. Chem. 10 (2017) S3358–S3366. doi:10.1016/j.arabjc.2014.01.016.
[103] H. Ashassi-Sorkhabi, Z. Ghasemi, D. Seifzadeh, The inhibition effect of some amino acids towards the corrosion of aluminum in 1M HCl+1M H2SO4 solution, Appl. Surf. Sci. 249 (2005) 408–418. doi:10.1016/j.apsusc.2004.12.016.
[104] S.A. Umoren, E.E. Ebenso, Studies of the anti-corrosive effect of *Raphia hookeri* exudate gum-halide mixtures for aluminium corrosion in acidic medium, Pigment Resin Technol. 37 (2008) 173–182. doi:10.1108/03699420810871020.
[105] I.M. Mejeha, M.C. Nwandu, K.B. Okeoma, L.A. Nnanna, M.A. Chidiebere, F.C. Eze, E.E. Oguzie, Experimental and theoretical assessment of the inhibiting action of Aspilia africana extract on corrosion aluminium alloy AA3003 in hydrochloric acid, J. Mater. Sci. 47 (2012) 2559–2572. doi:10.1007/s10853-011-6079-2.
[106] D. Wang, L. Gao, D. Zhang, D. Yang, H. Wang, T. Lin, Experimental and theoretical investigation on corrosion inhibition of AA5052 aluminium alloy by l-cysteine in alkaline solution, Mater. Chem. Phys. 169 (2016) 142–151. doi:10.1016/j.matchemphys.2015.11.041.
[107] A. Popova, E. Sokolova, S. Raicheva, M. Christov, AC and DC study of the temperature effect on mild steel corrosion in acid media in the presence of benzimidazole derivatives, Corros. Sci. 45 (2003) 33–58. doi:10.1016/S0010-938X(02)00072-0.
[108] I.B. Obot, N.O. Obi-Egbedi, S.A. Umoren, The synergistic inhibitive effect and some quantum chemical parameters of 2,3-diaminonaphthalene and iodide ions on the hydrochloric acid corrosion of aluminium, Corros. Sci. 51 (2009) 276–282. doi:10.1016/j.corsci.2008.11.013.
[109] K.B. Yatsimirskii, V.P. Vasil'ev, Instability Constants of Complex Compounds, Springer US, Boston, MA, 1995. doi:10.1007/978-1-4684-8404-5.
[110] S.M. Hassan, M.N. Moussa, M.M. El-Tagoury, A.A. Radi, Aromatic acid derivatives as corrosion inhibitors for aluminium in acidic and alkaline solutions, Anti-Corros. Methods Mater. 37 (1990) 8–11. doi:10.1108/eb007261.
[111] K.B. Sarangapani, V. Balaramachandran, V. Kapali, S. Venkatakrishna Iyer, M.G. Potdar, Aluminium as the anode in primary alkaline batteries, Surf. Technol. 26 (1985) 67–76. doi:10.1016/0376-4583(85)90112-8.

Figures

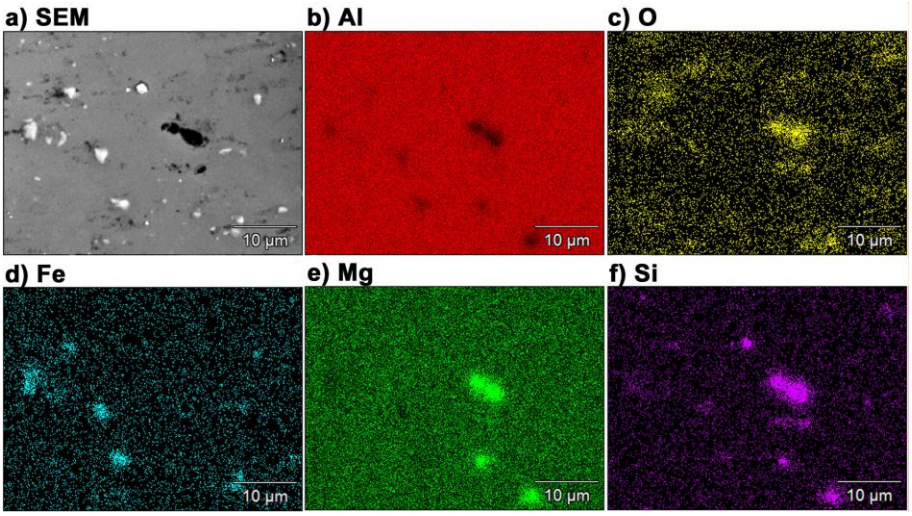

Fig. 1 - Energy dispersive X-Ray spectroscopy (EDS) chemical maps of as-polished AA5754 sample for aluminium, oxygen and main alloying additives. Accelerating voltage 20 kV. Magnification x2500.

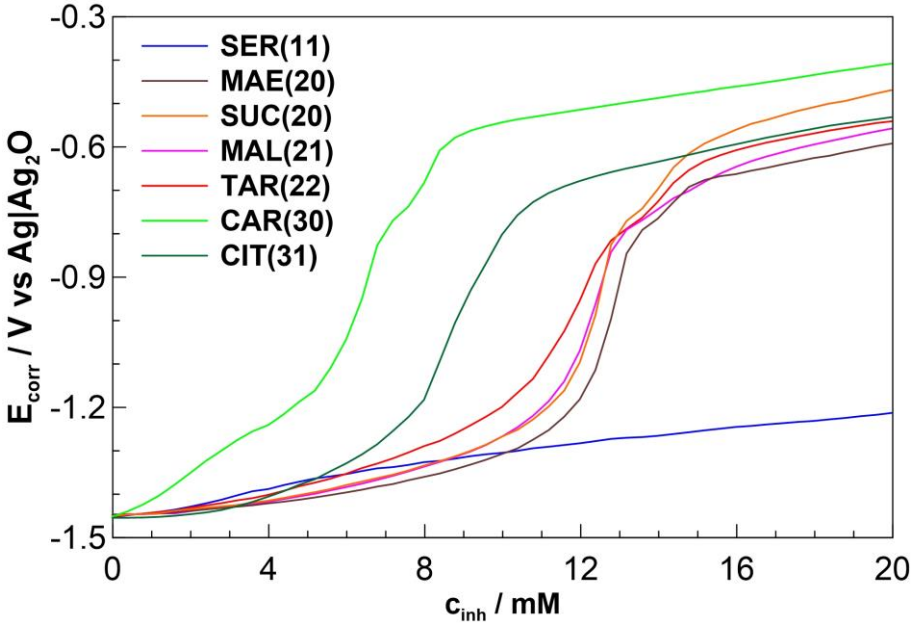

Fig. 2 – Changes in corrosion potential E_{corr} over time during the injection of investigated inhibitors into the bicarbonate buffer solution (pH 11). Measurements were carried out after 1000 s of initial sample conditioning. Average inhibitor injection rate was 0.37 mL/min.

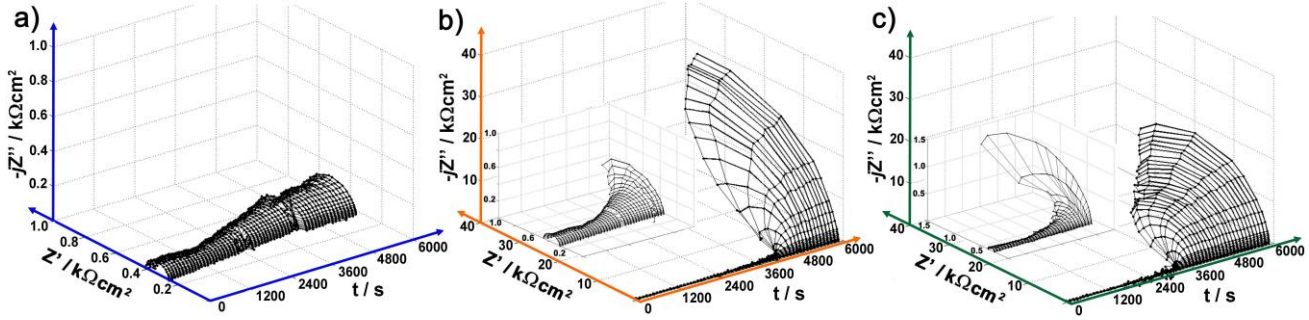

Fig. 3 – Instantaneous impedance spectra obtained by means of g-DEIS, drawn in Nyquist projection with time (increasing inhibitor concentration; average flow rate 0.37 mL/min) plotted on the Z-axis. Frequency range 4.5 kHz to 0.5 Hz. Samples: a) serine, b) succinic acid, c) citric acid.

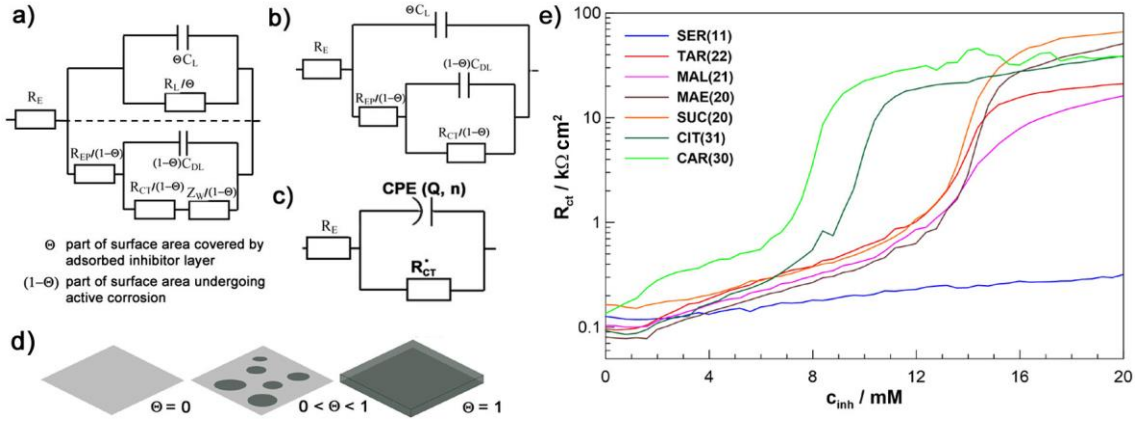

Fig. 4 – a) Electric equivalent circuit (EEC) and b,c) EEC simplified form used for the impedance data analysis, d) schematic representation of altering surface coverage and the formation of the adsorbed layer by the corrosion inhibitor molecules, e) instantaneous values of resultant charge transfer resistance R_{CT}, calculated by using R(QR) EEC. Measurements carried out in a bicarbonate buffer (pH 11) for various corrosion inhibitors.

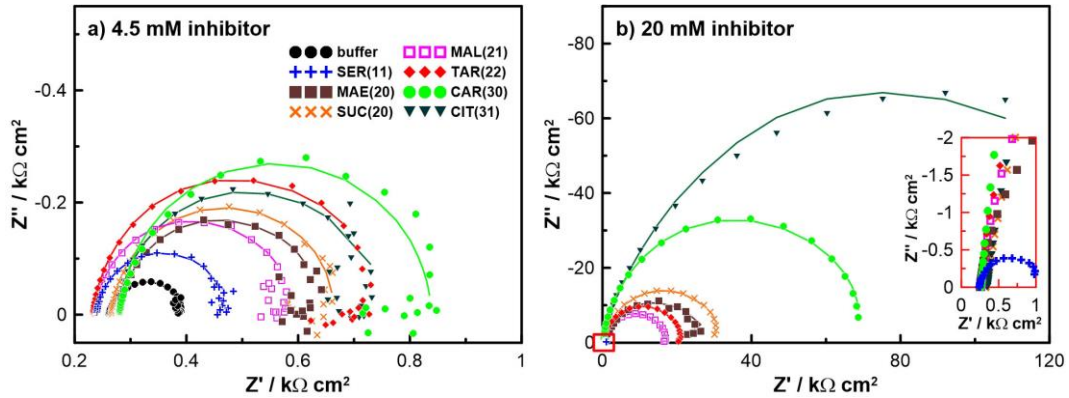

Fig. 5 – Classic EIS measurements for each investigated inhibitor compound in a bicarbonate buffer (pH 11), at the inhibitor concentration of a) 4.5 mM, and b) 20 mM. Points represent measured data, while the solid line has been approximated with R(QR) EEC applied in the frequency range between 100 kHz and 0.5 Hz.

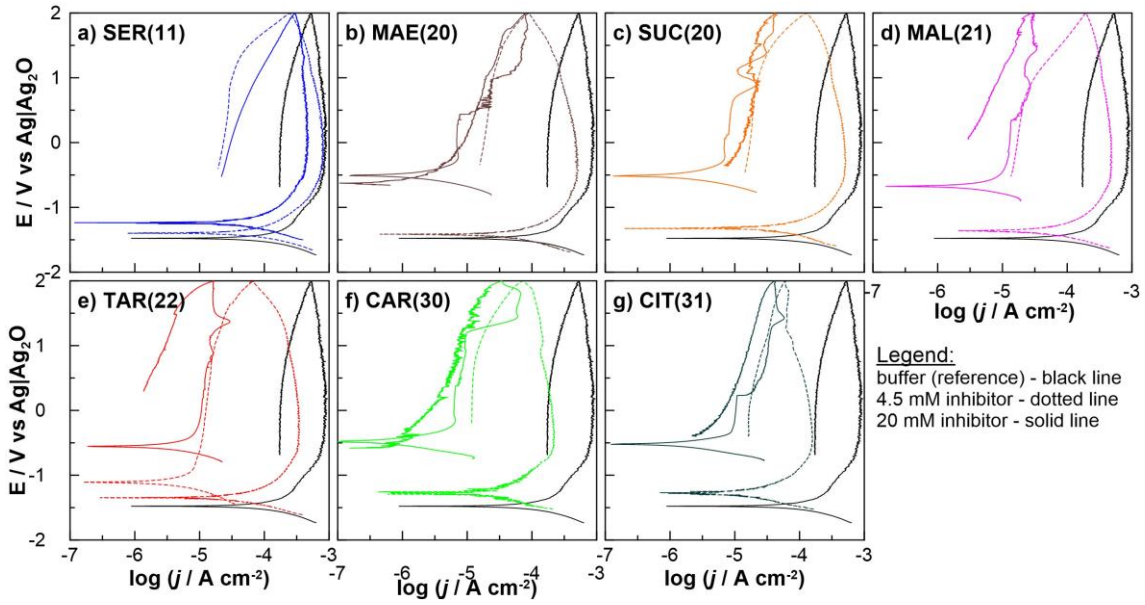

Fig. 6 – Cyclic polarization curves obtained for each investigated corrosion inhibitor (at concentrations of 0, 4.5 and 20 mM) mixed with bicarbonate buffer (pH 11). Polarization range from -0.25 vs E_{corr} to 2.00 V vs Ag|Ag_2O.

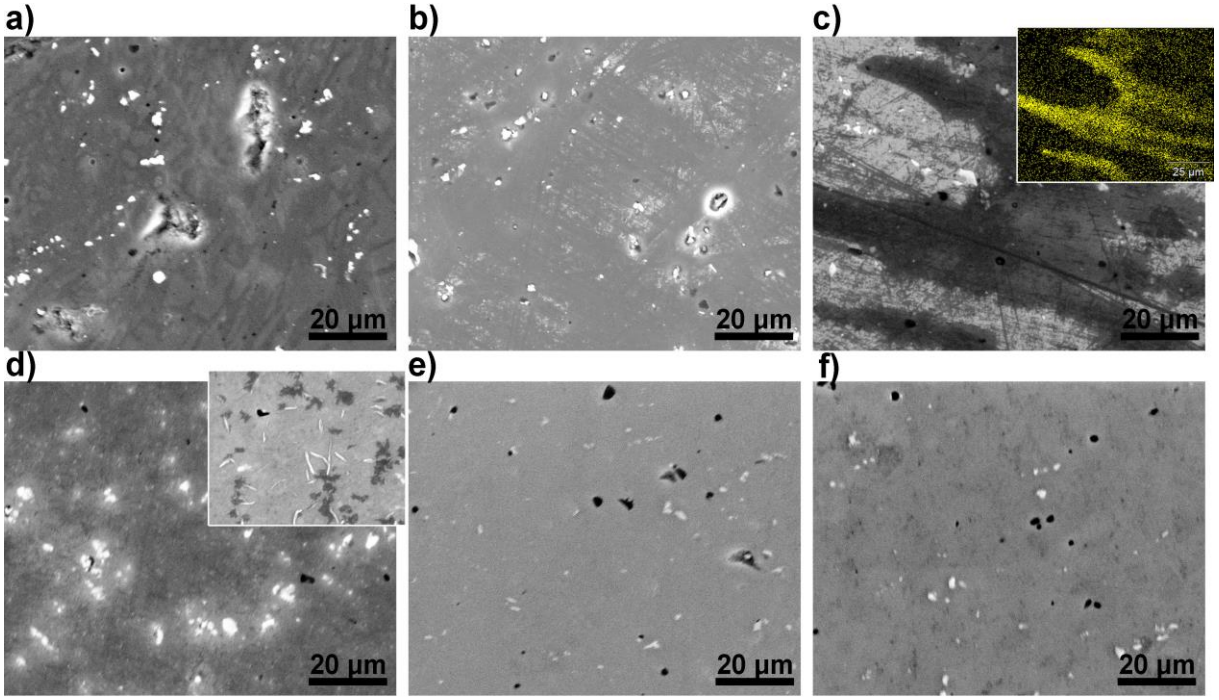

Fig. 7 – SEM micrographs of aluminium sample subjected for 6000 s to bicarbonate buffer (pH 11) with added carboxylic acids: a-c) 4.5 mM inhibitor, d-f) 20 mM inhibitor. a,d) serine, b,e) representative of dicarboxylic acids (succinic acid at 4.5 mM, and maleic acid at 20 mM); c,f) tricarboxylic acid (citric acid at 4.5 and 20 mM). Magnification x1000. In the inset: c) EDS chemical map of carbon for the investigated area, d) aluminium surface exposed to 100 mM serine.

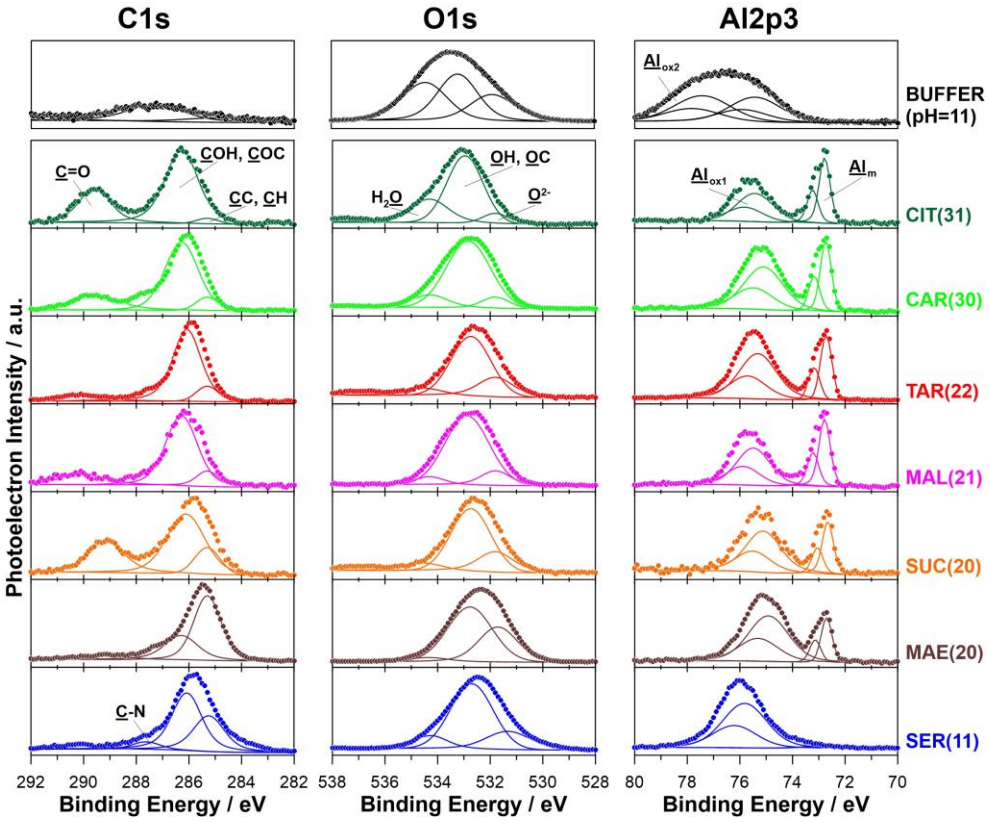

Fig. 8 – High-resolution XPS spectra obtained within the binding energy range (from left to right): *C1s*, *O1s* and *Al2p3* on the surface of aluminium samples exposed to bicarbonate buffer (pH 11) with admixed 20 mM of the investigated corrosion inhibitor. Superimposed sub-peaks represent the chemical states used during the deconvolution procedure.

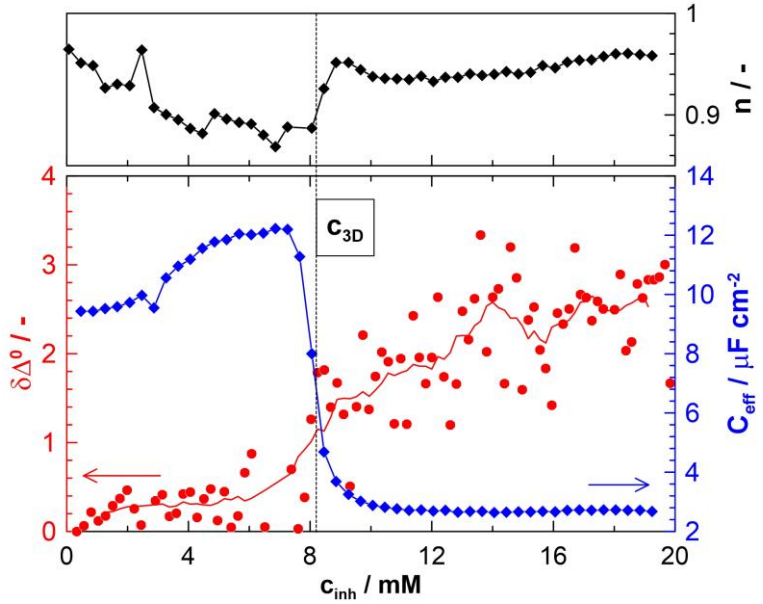

Fig. 9 – Impedance parameters C_{eff} and n, measured during the g-DEIS experiment, using R(QR) EEC and effective capacitance estimation for surface time-constant distribution, plotted against Δ^0 changes on the basis of ellipsometry measurement.

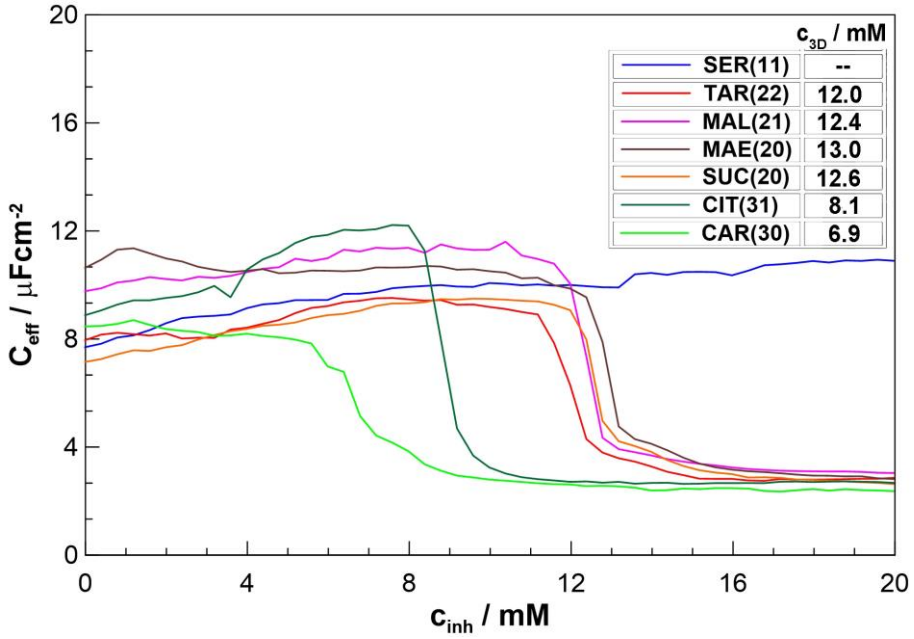

Fig. 10 – Changes in effective capacitance for each investigated carboxylic acid, estimated via Hirschorn's approach [96] for the surface distribution of capacitance dispersion. Data analyzed on the basis of g-DEIS measurements with R(QR) EEC. Table reveals the corrosion inhibitor concentration required for the formation of the adsorbed monolayer on the aluminium surface.

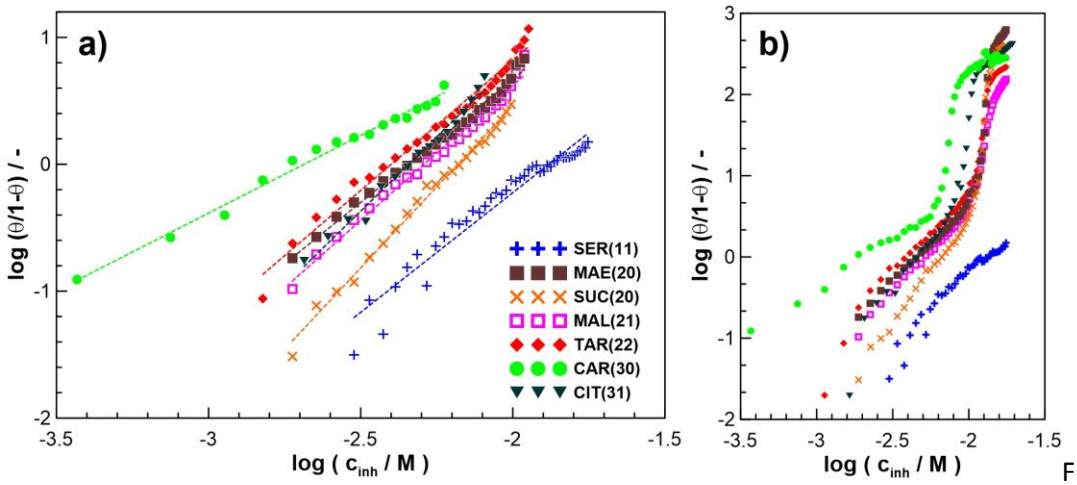

Fig. 11 – Adsorption isotherms based on the Langmuir adsorption model. Studies were carried out by using g-DEIS in bicarbonate buffer (pH 11): a) visualization of the results at the inhibitor concentration up to c_{3D} and b) for the full investigated concentration range. Average inhibitor injection rate was 0.37 mL/min.

Table 1 – The structural formulas of various carboxylic acids used in this study.

Common name	Systematic name	Acronym	Structural formula
DL-serine	DL-α-amino-β-hydroxyopropionic acid	SER(11)	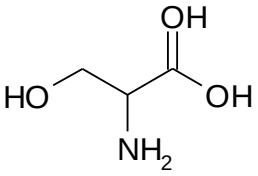
maleic acid	*cis*-butenedioic acid	MAE(20)	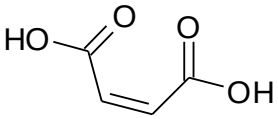
succinic acid	butanedioic acid	SUC(20)	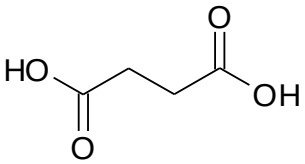
DL-malic acid	DL-2-hydroxybutanedioic acid	MAL(21)	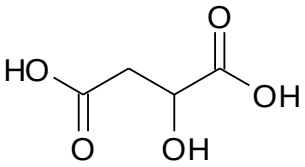
DL-tartaric acid	DL-1,2-dihydroxyethane-1,2-dicarboxylic acid	TAR(22)	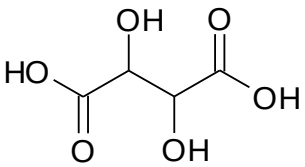
tricarballylic acid	propane-1,2,3-tricarboxylic acid	CAR(30)	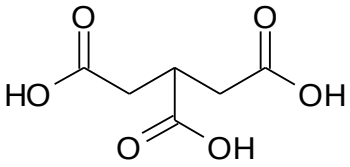
citric acid	2-hydroxypropane-1,2,3-tricarboxylic acid	CIT(31)	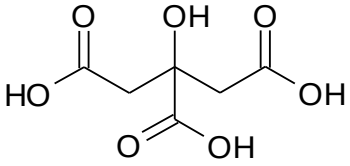

Table 2 – Corrosion inhibition efficiency estimated by using CP, EIS and g-DEIS after the exposure of aluminium samples to bicarbonate buffer (pH 11) containing admixed carboxylic acids as corrosion inhibitors.

Corrosion inhibitor	c / mM	CP		EIS		g-DEIS	
		j_{corr} / μA cm^{-2}	$IE_{\%}$ / %	R_{CT} / kΩ cm^2	$IE_{\%}$ / %	R_{CT} / kΩ cm^2	$IE_{\%}$ / %
BUFFER	0	111.0	-	0.13	-	0.12	-
SER (11)	4.5	47.4	57.3	0.23	43.5	0.15	20.0
	20	37.3	66.4	0.36	60.1	0.31	61.3
MAE (20)	4.5	38.7	65.1	0.36	63.5	0.16	25.0
	20	1.5	98.6	25.9	99.5	50.8	99.7
SUC (20)	4.5	46.6	58.0	0.41	67.5	0.23	47.8
	20	1.8	98.4	32.2	99.6	65.9	99.8
MAL (21)	4.5	45.6	58.9	0.35	62.6	0.18	33.3
	20	3.8	96.6	16.9	99.2	16.1	99.2
TAR (22)	4.5	34.3	69.1	0.51	74.1	0.22	45.5
	20	2.7	97.5	21.2	99.4	21.1	99.4
CAR (30)	4.5	16.0	85.6	0.59	77.5	0.48	75.0
	20	0.5	99.5	70.9	99.9	38.3	99.7
CIT (31)	4.5	17.2	84.5	0.46	71.3	0.20	40.0
	20	0.1	99.9	161.0	99.9	38.8	99.7

Table 3 – Surface chemical analysis (in at.%) based on XPS high-resolution measurements after spectral deconvolution.

Element		BE / eV	SER(11)*	MAE(20)	SUC(20)	MAL(21)	TAR(22)	CAR(30)	CIT(31)	REF
Al2p3	Al_m	72.7	1.3	4.5	4.4	11.0	10.8	8.1	9.2	--
	Al_{ox}	75.3	23.1	17.6	11.1	19.6	26.4	17.2	16.7	21.6
O1s	O^{2-}	531.7	11.5	13.9	9.5	5.2	10.7	4.0	2.6	18.0
	H_2O	534.4	3.9	1.6	3.5	2.7	2.6	4.1	4.7	24.4
	OH/CO	532.8	41.3	24.2	27.2	30.9	26.5	31.3	29.5	27.1
	**	OH	34.0	15.4	0.4	11.4	12.3	4.8	0.3	26.5
		CO	6.7	7.1	17.5	15.8	12.7	21.3	21.3	0.6
		C=O	0.6	1.7	9.3	3.7	1.5	5.3	7.9	--
C1s	C-C	285.1	5.9	23.0	4.6	2.8	1.0	1.5	0.8	0.5
	C-O	286.2	9.1	11.6	26.0	19.9	19.0	26.7	26.6	1.6
	C=O	289.3	0.8	2.9	13.7	4.6	2.3	6.7	9.9	--
Mg1	oxides	***	0.8	0.8	--	3.4	0.7	0.4	--	6.8

* serine sample had an additional contribution from C-N bonds, equal to 1.2 at.%; ** deconvolution of OH/CO peak to the individual contributions from OH, CO and C=O groups according to the model proposed by McCafferty and Wightman [83]; *** position of *Mg1s* peak is different for various compounds, and it ranges from 1304.3 to 1305.8 eV.

Table 4 - Gibbs free energy, ΔG estimated from adsorption isotherms using the Langmuir model of adsorption and g-DEIS measurement approach for the interaction between each investigated carboxylic acid and the aluminium surface exposed to a bicarbonate buffer (pH 11).

	SER(11)	MAE(20)	SUC(20)	MAL(21)	TAR(22)	CAR(30)	CIT(31)
ΔG / kJ mol^{-1}	-20.71	-21.00	-24.62	-21.86	-20.44	-16.85	-20.51